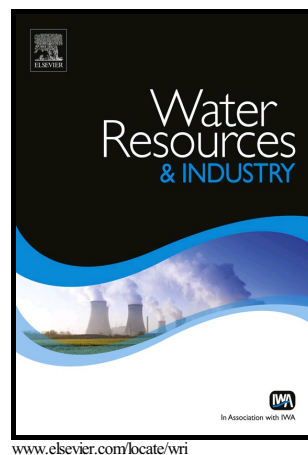


## Author's Accepted Manuscript

Development of iron oxide/activated carbon nanoparticle composite for the removal of Cr(VI), Cu(II) and Cd(II) ions from aqueous solution

Monika Jain, Mithilesh Yadav, Tomas Kohout, Manu Lahtinen, Vinod Kumar Garg, Mika Sillanpää



PII: S2212-3717(18)30071-4  
DOI: <https://doi.org/10.1016/j.wri.2018.10.001>  
Reference: WRI101

To appear in: *Water Resources and Industry*

Received date: 17 June 2018  
Revised date: 7 October 2018  
Accepted date: 10 October 2018

Cite this article as: Monika Jain, Mithilesh Yadav, Tomas Kohout, Manu Lahtinen, Vinod Kumar Garg and Mika Sillanpää, Development of iron oxide/activated carbon nanoparticle composite for the removal of Cr(VI), Cu(II) and Cd(II) ions from aqueous solution, *Water Resources and Industry*, <https://doi.org/10.1016/j.wri.2018.10.001>

This is a PDF file of an unedited manuscript that has been accepted for publication. As a service to our customers we are providing this early version of the manuscript. The manuscript will undergo copyediting, typesetting, and review of the resulting galley proof before it is published in its final citable form. Please note that during the production process errors may be discovered which could affect the content, and all legal disclaimers that apply to the journal pertain.

## Development of iron oxide/activated carbon nanoparticle composite for the removal of Cr(VI), Cu(II) and Cd(II) ions from aqueous solution

Monika Jain<sup>a,\*</sup>, Mithilesh Yadav<sup>b</sup>, Tomas Kohout<sup>c</sup>, Manu Lahtinen<sup>d</sup>, Vinod Kumar Garg<sup>e</sup> and Mika Sillanpää<sup>a</sup>

<sup>a</sup>Laboratory of Green Chemistry, Department of Chemistry, Lappeenranta University of Technology, Sammonkatu 12, FI-50130 Mikkeli, Finland

<sup>b</sup>Department of Chemical and Materials Engineering, Chang Gung University, 259, Wen-Hwa, 1st. Road, KweiShan, 33302, Taoyuan, Taiwan

<sup>c</sup>Department of Physics, University of Helsinki, P.O. Box 64, FI-40014, Finland

<sup>d</sup>Department of Chemistry, University of Jyväskylä, P.O. Box 35, FI-40014 JY, Finland

<sup>e</sup>Department of Environmental Science and Engineering, Guru Jambheshwar University of Science and Technology, Hisar, 125 001, Haryana, India

\*Corresponding author. Phone: +91-9891074838. monika.biorem@gmail.com

### Abstract

Iron oxide ( $\text{Fe}_3\text{O}_4$ ) and iron oxide/activated carbon ( $\text{Fe}_3\text{O}_4/\text{AC}$ ) were fabricated by co-precipitation method for the removal of Cr(VI), Cu(II) and Cd(II) ions from aqueous solution in batch mode. These nanoparticles were characterized by BET, FTIR, XRD, SEM/TEM and VSM. The optimum conditions for the removal of ions were pH=2 for Cr(VI) and 6 for Cu(II) and Cd(II), initial metal ion concentration=50mgL<sup>-1</sup>, nanoparticle dose=50mg/10mL, temperature=25±1°C, shaking speed=180 rpm and contact time=3h. The equilibrium data of ions sorption were well described by Langmuir, Freundlich, Redlich-Peterson and Intraparticle Diffusion model. The R<sup>2</sup> values obtained by Langmuir model were highest by  $\text{Fe}_3\text{O}_4/\text{AC}$  for Cr(VI)=0.9994, Cu(II)=0.9998 and Cd(II) = 0.9750. The temperature dependent study in the

range of 288 to 328 K confirmed that the adsorption process was endothermic in nature.

Desorption studies with 0.1 M HCl stated that these nanoparticles can be regenerated effectively and can be used after four adsorption-desorption cycles without any mass loss.

Graphical abstract

fx1

**Keywords:** Activated carbon; pH; XRD; TEM; iron oxide nanoparticles

## 1. Introduction

Today, water contamination with different pollutants (mainly heavy metals and dyes) has become a major environmental problem and a threat to the well being of living organisms [1-3]. Heavy metals are non-biodegradable, persistent, carcinogenic and toxic in nature and are widely distributed in the environment. They bioaccumulate in living organisms through food chain and their accumulation causes different diseases and malfunctions. Cadmium, chromium and copper are among few heavy metals that are discharged from several industrial effluents.

Cadmium is liberated into the environment from steel production, cement manufacture, Ni-Cd battery manufacture, cadmium electroplating, phosphate fertilizers etc. [4]. According to the World Health Organization (WHO) [5] guidelines, the maximum concentration for cadmium in drinking water was set at  $0.003 \text{ mg L}^{-1}$  in 2010. Zaini et al [6] reported that bivalent cadmium causes several deformities in humans such as muscular cramps, pulmonary problems, renal degradation, proteinuria, skeletal deformity, testicular atrophy etc.

Hexavalent chromium is another heavy metal in the environment released from various sources like electroplating, leather tanning, mining, textile and fertilizer industries. It is toxic, carcinogenic and mutagenic to human beings and animals [7-8]. It causes cancer in digestive

tract and lungs, epigastric pain, nausea, diarrhea, vomiting and hemorrhage as stated by Mohanty group [9]. The maximum permissible limit for hexavalent chromium in drinking water is  $0.05 \text{ mg L}^{-1}$  [10].

Copper is another essential element that is required for the synthesis of enzymes, tissues and bone development. The sources of copper from various industries include smelting, mining, electroplating, surface finishing, electric appliances, electrolysis and electrical components [11]. It is toxic and carcinogenic when ingested in large amounts and causes headache, vomiting, nausea, liver and kidney failure, respiratory problems and abdominal pain [12-13]. The maximum permissible limit set by USEPA for release of copper in industrial effluents is  $1.3 \text{ mg L}^{-1}$ . Thus, the effluents containing such kind of heavy metals which are harmful to living organism must be treated before discharging into ambient environment. In this regard, nanotechnology has been the focus of researchers since couple of years.

Iron oxide nanotechnology has been gaining the attraction of research society in solving the environment related problems [14-15]. This is because iron oxide is very useful in removing various kinds of air, water and soil contaminants through adsorption and photo-degradation. In addition to this, the deteriorating quality of water has led the researchers to use iron oxide nanoparticles as new generation adsorbents for water treatment [16]. Iron oxide is great adsorbent as it has high surface area-to-volume ratio, its surface can be modified, excellent magnetic properties, great biocompatibility, ease of separation using external magnetic field, reusability and comparatively low cost [17-18]. Also, it can coordinate with other elements due to variable oxidation states. Despite the above, iron oxide has one disadvantage that its particles aggregate due to their large surface-to-volume ratio and low surface energy [19-20]. To control this, surface modification is required to ensure the stability of particles.

Surface modification of iron oxide nanoparticles can be performed through coating, stabilization and functionalization. In surface coating, iron oxide attracts water molecules (hydrophilicity) and doesn't form clusters due the dispersion of particles [21]. The surface modification of iron oxide by activated carbon using coating technique improves their sorption capability because surface coating phenomenon helps in converting the closely - packed cubic geometry of magnetic nanoparticles into compact and strong [20]. Few examples can be found in the literature wherein the surface coated iron oxide nanoparticles have been utilized for the removal of heavy metals and dyes. Tailored EDTA di-anhydride treated magnetic  $\text{Fe}_3\text{O}_4$  baker's yeast biomass (EFB) was investigated by Xu et al. [22] for the removal of Pb(II) and Cd(II) ions from aqueous solution. Wannahari et al. [23] reported that sugarcane bagasse derived nanomagnetic adsorbent composite can remove Cu(II) from aqueous solution. Shen et al. [24] found that the adsorption capacity of iron oxide nanoparticles for the removal of Ni(II), Cu(II), Cd(II), Cr(VI) from contaminated water was high. Ghasemi group [19] reported high sorption capacity of surface coated iron oxide nanoparticles. Kakavandi group [25] studied the adsorption of Pb(II) onto  $\text{Fe}_3\text{O}_4$ /activated composite. Removal of dye from aqueous solution using  $\text{Fe}_3\text{O}_4$ -activated carbon nanocomposite was studied by Gholamvaisi et al [26]. Affam et al [27] found that the iron oxide/activated carbon composite can remove boron and organics from wastewater. In the similar way, it has also been found that [28-34] activated carbon/iron oxide composite is useful in removing different kinds of contaminants like trinitrophenol, phosphate, atrazine, lead, arsenic, mercury and methylene blue dye from aqueous solutions.

It is well-documented that, agricultural waste has huge scientific, social and economic significance as it is abundantly available at no or little cost, require simple processing, easy to handle and no regeneration is required. In 2013, our group [35] treated deseeded sunflower heads

with formaldehyde (to inhibit leaching of soluble organic matter from lignocellulosic materials). These treated sunflower heads (FSH) were then used for sequestering chromium ions from synthetic and steel industry wastewater. The adsorption capacity of FSH was found to be  $7.9 \text{ mg g}^{-1}$  for Cr(VI) at pH 2.0 and a temperature of  $25^\circ\text{C}$  from synthetic wastewater. While, the percent removal of Cr(VI), Cu(II) and Cd(II) from steel industry wastewater was 45, 40.8 and 35.1% respectively at their optimum pH i.e. 2.0, 5.0 and 6.0.

A review of literature on using sunflower and its parts (seed husk, seed hull, dried leaves, stalks) for the removal of heavy metals and dyes from wastewater revealed that very limited information is available. Some of the studies carried out by various researchers are given here in brief. Sun and Xu [36] investigated sunflower stalks for the removal of methylene Blue, Basic Red 9, Congo Red and Direct Blue 71 from aqueous solutions. Benaissa and Elouchdi [37] evaluated the potential of dried sunflower leaves for removing copper ions from single metal ion solution in a well-stirred batch reactor. Thinakaran et al [38] explored the adsorption of Acid Violet 17 using activated carbons prepared from sunflower seed hull (SSH) treated with sulphuric acid at three different temperatures. The adsorption efficiency of crushed and uncrushed sunflower husks for removal of methylene blue from aqueous solution was investigated by Soldatkina et al [39]. Sunflower stalks modified by nitric acid activation were used by Hussein [40] for the removal of copper from wastewater in batch and fixed bed mode. Activated carbon (via microwave induced  $\text{K}_2\text{CO}_3$  activation) was prepared by Foo and Hameed [41], from sunflower seed oil residue which is a by-product of sunflower seed oil refining industry. They utilized it for the removal of methylene blue and acid blue 15 from aqueous solution. The sunflower hulls are a waste material that originates from food industry. These hulls were used by Witek-Krowiak [42] for biosorption of Cu(II) ions from aqueous solution. Zou et al

[43] demonstrated that the activated carbon prepared from sunflower seed hull (an abundant agriculture byproduct) was highly porous, inexpensive and efficient adsorbent for removal of Cr(VI). Feizi and Jalali [44] explored sunflower stalks and leaves for the removal of Cd, Cu, Ni, Zn, Mn, Fe in single and competitive batch mode from aqueous solution. Saleh [3] prepared biochar from sunflower seed husk and found its adsorption potential in removing copper ions from wastewater. Srisorrachatr [45] prepared activated carbons from sunflower seed husks (SSH) by chemical activation with potassium carbonate and zinc chloride solution followed by carbonization and used them for removal of Pb(II), Ni(II), Zn(II) and Cd(II) from aqueous solution.

As it is clear from the review of literature that less research work has been carried out on unmodified sunflower head and stem waste. Besides this, only few studies have been reported on surface modification of iron oxide by using sun flower activated carbon for developing magnetic activated carbon nanocomposite. This combination has transformed the sunflower waste into useful magnetic activated carbon sorbents for removing toxic ions from wastewater. Another advantage is that the loaded adsorbents could be easily separated from the aqueous solution using magnet instead of centrifugation thus conserving energy.

Based on the aforementioned properties, agricultural waste (sunflower head waste) was chosen as a raw material which was combined with iron oxide nanoparticles as it was anticipated that this twofold combination of adsorption and magnetic separation would make the wastewater treatment process ecofriendly, effective and economically more attractive. In this study, material preparation, characterization and batch-type removal experiments were carried out wherein the feasibility of the above described composite for the removal of heavy metals [Cr(VI), Cu(II) and Cd(II)] from aqueous solution were investigated by varying the process conditions.

## Material and Methodology

### 2.1. Chemicals

All the chemicals used in this study were of analytical grade (Sigma Aldrich, FINLAND). Stock solutions of 1000 mg L<sup>-1</sup> concentration of Cd(NO<sub>3</sub>)<sub>2</sub>·4H<sub>2</sub>O, K<sub>2</sub>Cr<sub>2</sub>O<sub>7</sub> and Cu(NO<sub>3</sub>)<sub>2</sub>·3H<sub>2</sub>O were prepared in ultra-pure water acidified with nitric acid to prevent hydrolysis. The working solutions were made by diluting the stock solution. The pH of the solution was adjusted by adding 0.01M HCl or 0.01M NaOH and measured using electronic pH meter (WTW inoLab pH 730, Germany). The concentration of heavy metals in the aqueous solution was measured using Inductively Coupled Plasma Optical Emission Spectrometry (ICP-OES) [model iCAP 6000 (Thermo Electron Corporation, UK)] at a wavelength of 283.563 nm for Cr(VI), 324.75 nm for Cu(II) and 228.802 nm for Cd(II).

### 2.2. Preparation of nanoparticles

#### 2.2.1. Preparation of Activated Carbon by Sunflower Head Waste (chemical activation method)

Chemical activation can be carried by any of the mineral acids like HCl, HNO<sub>3</sub>, H<sub>2</sub>SO<sub>4</sub>, phosphoric acid as it increases the porosity of the carbon structure during the acid treatment. Impregnation ratio also strongly affects the characteristics of activated carbon (AC). As our's was an agricultural waste, so it contained large amount of lignin and if the percentage of lignin is more, then sulphuric acid activation leads to an increase in BET surface area [46].

Table 1 depicts that, the surface area, pore volume and pore width, all increased after activation with sulphuric acid, as this process leads to an extensive increase in the porosity of the

material (Fig. 5). If we compare the surface area of the ACs prepared by sulphuric acid, phosphoric acid, zinc chloride, then, it was found that the surface area of sulphuric acid treated AC was highest [47]. High surface area and pore structure are the basic parameters for an effective adsorbent and these parameters are introduced by chemical activating agents like sulphuric acid.

Activated Carbon prepared from sunflower head waste was synthesized as per the method reported by [48]. Sunflower head waste biomass was crushed into fine powder in a steel mill. Crushed powder was boiled in distilled water and cooled. The procedure of boiling and cooling was repeated till the supernatant was colorless. The washed crushed powder was rinsed with 1% HCl, washed again with distilled water till the wash water became colorless. The powder was dried at 80 °C for 24h in a hot air oven to get rid of moisture and volatiles. Pretreated sunflower head waste powder was treated with concentrated sulphuric acid in the ratio of 1:2 (w/v). It was then washed with distilled water continuously to remove free acid and soaked in 1% sodium bicarbonate solution overnight to neutralize the acid. It was then washed with distilled water and dried at 80 °C in hot air oven for 24h. The dried material was subjected to thermal activation in a muffle furnace at 500 °C flushed with nitrogen gas at a flow rate of 20 mL min<sup>-1</sup> for 1.0 h. The material was cooled in N<sub>2</sub> atmosphere, washed with ultra-pure water and dried at same conditions as mentioned above. The activated carbon (namely AC) was sieved from the standard mesh of size 250 µm and stored in a vacuum desiccator for further use.

### 2.2.2. Preparation of Iron oxide/Activated Carbon nanocomposite (Fe<sub>3</sub>O<sub>4</sub>/AC) and Iron Oxide Nanoparticles (Fe<sub>3</sub>O<sub>4</sub>)

The Iron oxide/Activated Carbon nanocomposite (Fe<sub>3</sub>O<sub>4</sub>/AC) was prepared as reported by [14] with some modification. A required amount of AC was dispersed in 400 mL solution of

7.8 g of  $\text{FeCl}_3 \cdot 6\text{H}_2\text{O}$  (28 mM) and 3.8 g of  $\text{FeSO}_4 \cdot 7\text{H}_2\text{O}$  (14 mM) with vigorous stirring on a magnetic stirrer at 700 rpm at 70–80 °C. The NaOH (5.0 M) solution was added drop wise into the above suspension under vigorous stirring at 80 °C until pH raised to 10-11 to precipitate the hydrated iron oxide. The suspension was stirred further on a magnetic stirrer at 80 °C for 1.0 h. Next, it was aged at room temperature for 24h. The  $\text{Fe}_3\text{O}_4/\text{AC}$  nanocomposite were separated by a magnet and washed repeatedly with distilled water and ethanol till neutral pH. They were then dried in hot air oven at 80 °C for 12h. After drying, the nanoparticles were crushed in mortar and pastel and stored in air tight plastic containers for further use. In addition, the procedure for synthesis of iron oxide nanoparticles ( $\text{Fe}_3\text{O}_4$ ) was similar as mentioned above except that no AC was added.

### 2.3. Characterization of nanoparticles

#### 2.3.1. Surface area analysis

The BET surface area and pore volume of the nanoparticles were measured BJH desorption method in  $\text{N}_2$  atmosphere at 77 K in a Quantachrome surface area analyzer (model Autosorb 1). The nanoparticles before measurement were degassed at 200 °C for 24h in order to remove the moisture.

#### 2.3.2. pH – Point Zero Charge ( $\text{pH}_{\text{pzc}}$ )

The  $\text{pH}_{\text{pzc}}$  was measured using 0.01M NaCl aqueous solution. The initial pH of the solution was set in the range of 2 -12 with 0.1M HCl/NaOH and 50 mL of this solution was added to the conical flasks containing 0.15 g of  $\text{Fe}_3\text{O}_4$  and  $\text{Fe}_3\text{O}_4/\text{AC}$ . The flasks were agitated in an orbital shaker for 48h and the final pH of the solution was determined using pH meter. The value of  $\text{pH}_{\text{pzc}}$  was obtained by plotting the graph between  $\text{pH}_{\text{final}}$  versus  $\text{pH}_{\text{initial}}$ . The point of intersection of  $\text{pH}_{\text{final}}$  versus  $\text{pH}_{\text{initial}}$  was the  $\text{pH}_{\text{pzc}}$  of the nanoparticles.

### 2.3.3. Fourier Transform Infrared Spectroscopy (FT-IR)

FT-IR spectra of native as well as Cr(VI), Cu(II) and Cd(II) loaded magnetic nanoparticles was recorded using FT-IR Spectrometer (BRUKER OPTIK GmbH, FT-IR Spectrometer VERTEX 70, Germany) between 4500 to 400  $\text{cm}^{-1}$  at a resolution of 4.0  $\text{cm}^{-1}$  taking 32 scans for each spectrum.

### 2.3.4. Powder X-Ray Diffraction studies (PXRD)

The diffraction data for the examined  $\text{Fe}_3\text{O}_4$  and  $\text{Fe}_3\text{O}_4/\text{AC}$  samples were acquired using powder X-Ray diffractometer (PAN analytical X'Pert PRO alpha 1) with monochromatic  $\text{Cu-K}_{\alpha 1}$  radiation (primary beam Johansson monochromator;  $\lambda = 1.5406 \text{ \AA}$ ) at 45 kV and current of 30 mA. Data were recorded with position sensitive X'Celerator detector in a continuous scanning mode:  $2\theta$ -range of 10 - 70° with a step size of 0.017°. Diffraction patterns were processed with PANalytical High Score Plus program (v. 4.5). Scherrer equation (1) was used for calculating the average crystal size of magnetic nanoparticles:

$$D = \left( \frac{k\lambda}{\beta \cos \theta} \right) \quad (1)$$

where D = average size of the crystals; K = shape-dependent Scherrer's constant (0.90);  $\lambda$  = radiation wavelength (1.5406  $\text{\AA}$ );  $\beta_s$  = full width at half maximum intensity (FWHM given in radians);  $\theta$  = Braggs diffraction angle.

### 2.3.5. Scanning Electron Microscopy (SEM) and Energy Dispersive X-ray Spectroscopy (EDS)

The texture and surface morphology of  $\text{Fe}_3\text{O}_4$  and  $\text{Fe}_3\text{O}_4/\text{AC}$  were determined using a field emission Scanning Electron Microscope (model HITACHI S-4800) at an accelerating voltage of 30 KV with a working distance of 8.0 mm and an emission current of 20.0

microamperes of Tungsten filament. The SEM images were obtained at a magnification of 400 k. The elemental composition of the samples was obtained using Energy Dispersive X-ray Spectrometer (model EDAX TSL AMETEK, USA) in conjunction with SEM.

#### 2.3.6. Transmission Electron Microscopy (TEM)

The particle size of the nanoparticles was determined using high-resolution aberration-corrected Transmission Electron Microscope (model JEOL-2200FS, Japan) operated at 200 kV. For sample preparation, the nanoparticles were dispersed in acetone for 30 min in a sonicator. The samples were then dropped on standard holey carbon films and dried at room temperature. They were then transferred to Cu grids (Agar Scientific, UK) for analysis in the microscope.

#### 2.3.7. Magnetic properties (Vibrating Sample Magnetometer)

The magnetic hysteresis and susceptibility measurement of magnetic nanoparticles were measured using Vibrating Sample Magnetometer (Princeton Measurements Micromag Model 3900 VSM, USA) at room temperature at a maximum applied magnetic field of 1.2 Tesla.

#### 2.3.8. Thermogravimetric analysis (TGA)

The changes in the mass of  $\text{Fe}_3\text{O}_4$  and  $\text{Fe}_3\text{O}_4/\text{AC}$  as a function of temperature in a defined and controlled environment from 26 to 1000 °C were measured by TGA/DTG curves in  $\text{N}_2$  atmosphere at a heating rate of 20 °C  $\text{min}^{-1}$  (model NETZSCH TG 209F1 220-10-155-K, Germany).

### 3. Batch adsorption studies

The batch mode adsorption experiments were conducted to evaluate the removal of Cr(VI), Cu(II) and Cd(II) ions from aqueous solutions. For the adsorption experiments, 10 mL solution of each ion of desired concentration (10 to 500  $\text{mg L}^{-1}$ ) at a predetermined initial pH

[2.0 Cr(VI), 6.0 Cu(II) and Cd(II)] and nanoparticle dosage in 15 mL disposable, capped tubes at  $26\pm 1$  °C at an agitation speed of 180 rpm in a rotary shaker (model temperature controlled IKA KS 4000 ic, Germany) were agitated for 24h. The nanoparticles were separated by strong magnet and the supernatant was collected by 0.20  $\mu\text{m}$  polypropylene membrane syringe filter. Residual concentration of the metal ions in the solution was determined using Inductively Coupled Plasma Optical Emission Spectrometry (ICP-OES). The percent metal removal (R %) was calculated using equation 2:

$$R(\%) = \frac{C_i - C_e}{C_i} \times 100 \quad (2)$$

where  $C_i$  and  $C_e$  were the initial and equilibrium concentration of metals in the solution. The adsorption capacity ( $q_e$ ) of the nanoparticles at equilibrium time was calculated using equation 3:

$$q_e (\text{mg/g}) = \left[ \frac{C_i - C_e}{M} \right] \times V \quad (3)$$

where  $C_i$  and  $C_e$  are same as above.  $V$  is the volume of solution (L) and  $M$  is the mass of nanoparticles (in g) used.

## 4. Results and Discussion

### 4.1. Characterization of nanoparticles

The data indicated that, the Sunflower Head Waste (SHW) has a very small surface area ( $0.99 \text{ m}^2 \text{ g}^{-1}$ ) with a pore volume of  $0.0007 \text{ cm}^3 \text{ g}^{-1}$  (Table 1). While, when SHW was converted into activated carbon (AC), the surface area increased to  $25.07 \text{ m}^2 \text{ g}^{-1}$ . The surface area of  $\text{Fe}_3\text{O}_4$  was found to be  $47.87 \text{ m}^2 \text{ g}^{-1}$  that further increased to  $51.1 \text{ m}^2 \text{ g}^{-1}$  when  $\text{Fe}_3\text{O}_4$  was coated with AC. The  $\text{pH}_{\text{pzc}}$  (pH at point of zero charge) of  $\text{Fe}_3\text{O}_4$  and  $\text{Fe}_3\text{O}_4/\text{AC}$  was found to be 5.2 and 7.04 respectively.

Adsorbents with diverse type of chemical groups like carboxyl, hydroxyl, ester, aldehyde, ketone etc. have the ability to bind with metal ions. Their affinity for metal uptake depends on factors like the number of sites, their accessibility, chemical form, affinity between binding sites and metal ions etc. [49]. The functional groups and their corresponding frequencies are shown in the FT-IR spectra of  $\text{Fe}_3\text{O}_4$  and  $\text{Fe}_3\text{O}_4/\text{AC}$  and metal loaded  $\text{Fe}_3\text{O}_4$  and  $\text{Fe}_3\text{O}_4/\text{AC}$  (<sup>P</sup>Fig.1). FTIR analysis indicated the presence of several strong absorption peaks. The presence of infrared absorption peaks at about 530.35, 528.42, 522.64, 568.21  $\text{cm}^{-1}$  in  $\text{Fe}_3\text{O}_4$ , Cr, Cu and Cd loaded  $\text{Fe}_3\text{O}_4$  and 536.14, 534.29, 538.07, 530.67  $\text{cm}^{-1}$  in  $\text{Fe}_3\text{O}_4/\text{AC}$ , Cr, Cu and Cd loaded  $\text{Fe}_3\text{O}_4/\text{AC}$  respectively confirmed the presence of iron oxide nanoparticles with respect to characteristic stretching band of Fe–O onto their surface [24]. No other peak was found in  $\text{Fe}_3\text{O}_4$  thus, indicating that it comprised of iron oxide only.

On the other hand, in  $\text{Fe}_3\text{O}_4/\text{AC}$ , the peak at 2341.29  $\text{cm}^{-1}$  is attributed to aromatic  $-\text{C}=\text{C}$ . The strong  $-\text{C}-\text{O}$  band at 1037.57  $\text{cm}^{-1}$  due to  $-\text{OCH}_3$  group is due to the presence of lignin structure in the sunflower head which is the characteristic peak of polysaccharides. The band at 1585.28  $\text{cm}^{-1}$  in chromium loaded  $\text{Fe}_3\text{O}_4/\text{AC}$  may be due to asymmetric stretching of  $-\text{C}-\text{O}$  bond, stretching of aromatic  $-\text{C}=\text{C}$  bond or due to amide stretching. In copper, loaded  $\text{Fe}_3\text{O}_4/\text{AC}$ , the absorption peak at 3423.22  $\text{cm}^{-1}$  may be attributed to  $-\text{NH}/-\text{OH}$  stretching indicating the existence of free and intermolecular bonded hydroxyl group due to alcoholic or phenolic functions and amine group. The peak around 1612.28  $\text{cm}^{-1}$  corresponds to  $-\text{C}=\text{O}$  stretching that may be attributed to lignin aromatic group. Similarly, in cadmium loaded  $\text{Fe}_3\text{O}_4/\text{AC}$ , the peaks shifted as compared to native nanoparticles (<sup>P</sup>Fig. 1). The additional peaks at 869.78  $\text{cm}^{-1}$  and 781.07  $\text{cm}^{-1}$  in  $\text{Fe}_3\text{O}_4/\text{AC}$  and Cr(VI) loaded  $\text{Fe}_3\text{O}_4/\text{AC}$ ; 862.5  $\text{cm}^{-1}$  in Cu(II) loaded  $\text{Fe}_3\text{O}_4/\text{AC}$ ;

875.57  $\text{cm}^{-1}$  and 767.57  $\text{cm}^{-1}$  in Cd(II) loaded  $\text{Fe}_3\text{O}_4/\text{AC}$  may be assigned to bending modes of aromatic compounds.

These changes indicated that the carboxyl, amino/hydroxyl groups present on the surface of native and metal loaded  $\text{Fe}_3\text{O}_4/\text{AC}$  are mainly involved in the adsorption of metal ions. The possible adsorption on these nanoparticles may be due to physical adsorption, complexation with functional groups [18, 50], ion exchange [51], surface precipitation or chemical reaction with surface sites. The changes in FTIR spectra confirm the complexation of Cr(VI), Cu(II) and Cd(II) with functional groups present on the nanoparticles.

Comparison of powder X-ray diffraction (PXRD) patterns of  $\text{Fe}_3\text{O}_4$  and  $\text{Fe}_3\text{O}_4/\text{AC}$  (Fig.1) samples revealed that the iron oxide nanoparticles in both samples are crystalline in nature and represent cubic structure modification of  $\text{Fe}_3\text{O}_4$  (magnetite), as characteristic diffraction peaks (with corresponding Miller indices) can be observed e.g. at  $2\theta$  of  $30.18^\circ$  (220),  $35.54^\circ$  (311),  $43.21^\circ$  (400),  $54.00^\circ$  (422),  $57.16^\circ$  (511) and  $62.78^\circ$  (440), respectively (Table 2). As all the observed peaks, can be assigned by the magnetite phase, no peaks for the potential hematite phase can be seen in either of the patterns. In addition, a very weak, broad diffraction hump at  $2\theta$  range of  $23^\circ$  was observed in case of  $\text{Fe}_3\text{O}_4/\text{AC}$  sample, confirming presence of activated carbon on the surfaces of magnetic nanoparticles [35]. The crystal size analysis with Scherrer equation indicated nearly the same crystal size of both the magnetite nanoparticles (~15 to 21 nm in diameter depending on the direction of the view of the crystal lattice).

The SEM micrographs of  $\text{Fe}_3\text{O}_4$ ,  $\text{Fe}_3\text{O}_4/\text{AC}$ , Cr, Cu & Cd loaded  $\text{Fe}_3\text{O}_4$  and Cr, Cu & Cd loaded  $\text{Fe}_3\text{O}_4/\text{AC}$  are shown in Fig. 2. SEM images give an idea about the shape and structure of the nanoparticles under study. AC has a tubular and porous structure (Fig. 5 a & b) with smooth

surface while images of  $\text{Fe}_3\text{O}_4$  and  $\text{Fe}_3\text{O}_4/\text{AC}$  (Fig. 2 a and e) reveal that the nanoparticles are agglomerated and stuck to each other thus, making the surface rough and coarse. The surface of the nanosorbents after loading with heavy metals (Fig. 2 b, c, d, f, g and h) became smooth and shiny as visible in the images. The adsorption of heavy metals on the surface of nanoparticles was further confirmed by EDS. Detailed morphology and structure of the nanoparticles was further investigated by TEM.

As can be seen in the EDS spectra of  $\text{Fe}_3\text{O}_4$  sample (Fig. 3a), it does not contain carbon and weight fraction of iron is 63.8% whereas in  $\text{Fe}_3\text{O}_4/\text{AC}$  (Fig. 3e), the weight fraction of carbon is 50.9% and iron content is only 18.4% confirmed by the sharp peaks of carbon and iron thus, indicating that the activated carbon content was significantly higher than  $\text{Fe}_3\text{O}_4$  NPs. Moreover, E

DS spectrum of  $\text{Fe}_3\text{O}_4/\text{AC}$  sample showed an additional peak that could be assigned to silicon that might have originated from the plant material. Partial images of b, c, d, f, g and h in Fig. 3 corresponds to the EDS spectra of  $\text{Fe}_3\text{O}_4$  and  $\text{Fe}_3\text{O}_4/\text{AC}$  after loading with Cr, Cu and Cd respectively. The characteristic peaks of Cr, Cu and Cd in the spectra revealed that the metal ions bonded well with the surface of the nanoparticles.

TEM images of synthesized  $\text{Fe}_3\text{O}_4$  and  $\text{Fe}_3\text{O}_4/\text{AC}$  nanoparticles along with the particle size distribution (in the inset i.e. Selected Area Diffraction Pattern) are given in Fig.4 a, b, c and d. The nanoparticles synthesized by co-precipitation method are nearly spherical in shape with an average particle size of 12.9 nm ( $\text{Fe}_3\text{O}_4$ ) and 12.3 nm ( $\text{Fe}_3\text{O}_4/\text{AC}$ ). The particle size of  $\text{Fe}_3\text{O}_4$  and  $\text{Fe}_3\text{O}_4/\text{AC}$  was in the range of 7 to 19 nm and 9 to 18 nm respectively, thereby being consistent with XRD analysis (see earlier paragraph of same section).

The magnetic hysteresis loop of iron oxide nanoparticles (Fig. 6) was plotted between field strength (T) and ratio of magnetic moment to mass [ $J(\text{Am}^2 \text{kg}^{-1})$ ]. The saturation magnetization i.e.  $J_s$  [ $(\text{Am}^2 \text{kg}^{-1})$ ] that measures the maximum magnetic strength was found to be 59.3 and 52.2  $\text{Am}^2/\text{kg}$  respectively for  $\text{Fe}_3\text{O}_4$  and  $\text{Fe}_3\text{O}_4/\text{AC}$  (Table 3).  $J_s$  values obtained for both the nanoparticles is lesser than the pure magnetite ( $\text{Fe}_3\text{O}_4$ ) i.e. 92  $\text{Am}^2 \text{kg}^{-1}$  [52]. Although both the nanoparticles are quite similar in their magnetic properties but  $\text{Fe}_3\text{O}_4/\text{AC}$  has less saturation magnetization due to the presence of plant biomass in it (Table 3). However, this reduction in magnetization did not affect the attraction by external magnet as  $\text{Fe}_3\text{O}_4/\text{AC}$  was still strongly attracted by the external magnet. The coercivities [ $H_c$  (mT)] of  $\text{Fe}_3\text{O}_4$  and  $\text{Fe}_3\text{O}_4/\text{AC}$  are 5.2 and 3.6 T respectively indicating that the nanoparticles are of ferromagnetic nature (Table 3). The remnant magnetization ( $J_r$ ), a measure of the remaining magnetization when the driving field is dropped to zero is 5.3 and 4.0 ( $\text{Am}^2 \text{kg}^{-1}$ ) for  $\text{Fe}_3\text{O}_4$  and  $\text{Fe}_3\text{O}_4/\text{AC}$  respectively (Table 3). Thus,  $\text{Fe}_3\text{O}_4$  and  $\text{Fe}_3\text{O}_4/\text{AC}$  with high saturation magnetization values can quickly respond to the external magnetic field thereby leading to their fast separation from the aqueous solution of heavy metal. The data indicated that both the specimens show similar hysteresis parameters (Table 3 and Fig. 6).

The TGA/DTG analysis was performed to identify the thermal behavior and stability of the nanoparticles in the nitrogen atmosphere. TGA was used to determine the thermal stability of  $\text{Fe}_3\text{O}_4$  and  $\text{Fe}_3\text{O}_4/\text{AC}$  by monitoring the weight change that occurred when the samples were heated in an inert atmosphere of  $\text{N}_2$ . Fig.7. showed the mass loss (TGA) and derivative mass loss (DTG) curves of  $\text{Fe}_3\text{O}_4$  and  $\text{Fe}_3\text{O}_4/\text{AC}$ .

In Fig.7,  $\text{Fe}_3\text{O}_4$  showed two step degradation as indicated by the DTG peaks. The observed maximum weight loss occurred at first peak i.e. at around 65 °C which was attributed

to the loss of moisture. The second peak at 270°C in the temperature range of 175-400 °C, with a further weight loss of 1.7% corresponded to the removal of chemically bound moisture. Above 400 °C, only negligible change in mass (<0.55%) was observed indicating that no further reactions occurred until 1000 °C thereby iron oxide being the sole residue with residual mass of 96% at the end of the degradation.

On the other hand, the degradation of Fe<sub>3</sub>O<sub>4</sub>/AC occurred in four distinct stages as indicated by the DTG peaks. The first weight loss (below 175 °C) was mainly due to the loss of moisture. A second peak at around 276 °C with very low weight loss (within 175 to 387 °C) was found due to the thermal degradation of cellulose and hemicellulose [53]. Between 387-787 °C, a third peak with a loss of 8.4% was due to the devolatilization of more thermally stable heavy volatiles present in Fe<sub>3</sub>O<sub>4</sub>/AC [54]. The fourth stage was from 787 to 969 °C, in which the slow weight loss was due to the pyrolysis of lignin in biomass [55-57]. At the end of temperature (999.2 °C), the final residual mass of 77.7% was identified which might be the representative of materials including iron oxide and some other carbonaceous residuals.

## 4.2. Batch adsorption studies

### 4.2.1. pH dependent studies

The effect of pH (Fig. 8 a, b, c and d) on the adsorption of Cr(VI), Cu(II) and Cd(II) ions by Fe<sub>3</sub>O<sub>4</sub> and Fe<sub>3</sub>O<sub>4</sub>/AC was studied in order to determine the optimum adsorption pH of the above said ions in the pH range of 2.0-7.0. While screening the pH values, all the other process variables such as initial metal ion concentration (50 mg L<sup>-1</sup>), nanoparticle dose (50 mg/10 mL), temperature (26±1 °C), shaking speed (180 rpm) and contact time (3 h) were kept constant. A control experiment was also run (in the absence of nanoparticles) for the removal of Cr(VI),

Cu(II) and Cd(II) to explore the effect of chemical precipitation (Fig. 8 c). Performed control experiment revealed that there was no removal of Cr(VI) & Cd(II) up to pH 7.0 and Cu(II) up to pH 6.0 but when the pH was  $>6.0$  [(for Cu(II))] and  $>7.0$  [for Cd(II) and Cr(VI)], all the three ions precipitated as hydroxides [ $\text{Cr}(\text{OH})_2$ ,  $\text{Cu}(\text{OH})_2$  and  $\text{Cd}(\text{OH})_2$ ] in the solution thus, leading to their complete removal. Keeping this in view, the adsorption studies were conducted in the pH range of 2.0 – 7.0 for Cr(VI) and Cd(II) and 2.0 – 6.0 for Cu(II), as Cu(II) precipitated at pH 7.0 and Cr(VI) and Cd(II) precipitated at pH 8.0.

Fig. 8a and b display that maximum removal of Cr(VI) was achieved at pH 2.0 and that of Cu(II) and Cd(II) was at pH 6.0. In case of  $\text{Fe}_3\text{O}_4$ , it was observed that, Cr(VI) removal decreased (58.5 to 11.6%) as pH was increased from 2.0 to 7.0. Whereas Cu(II) and Cd(II) removal increased from 0 to 26.2% and 2.6 to 8.4% respectively when the pH was increased from 2.0 to 6.0. While the percentage removal decreased from 95.3 to 10.3 % in case of Cr(VI), it increased from 0 to 85.6% and from 5.5 to 96.5% for Cu(II) and Cd(II) respectively when  $\text{Fe}_3\text{O}_4/\text{AC}$  was used in the given pH range indicating higher removal efficiency of  $\text{Fe}_3\text{O}_4/\text{AC}$  over  $\text{Fe}_3\text{O}_4$ . It can be assumed that it was the presence of different functional groups on the surface of activated carbon that led to increased binding of more ions as suggested by Jain et al [49].

One way to explain the mechanism of Cr(VI) removal is that, at lower pH, the surface of the nanoparticle is positively charged due to adsorption of  $\text{H}^+$  ions from the aqueous solution. The chromium ions co-exist in different forms viz.  $\text{HCrO}_4^-$ ,  $\text{Cr}_2\text{O}_7^{2-}$ ,  $\text{Cr}_3\text{O}_{10}^{2-}$ ,  $\text{Cr}_4\text{O}_{13}^{2-}$  of which  $\text{HCrO}_4^-$  predominates in the pH range of 1.0 - 6.0 and chromate ions ( $\text{CrO}_4^{2-}$ ) exists at pH  $>6.0$  [58]. This leads to an electrostatic attraction between the positively charged nanoparticles surface and negatively charged chromate ions thus, leading to an increase in the removal at lower pH

(pH=2.0) (**Scheme I**). The decrease in removal at higher pH may be due to competition between chromate ( $\text{CrO}_4^{2-}$ ) and hydroxyl ions ( $\text{OH}^-$ ) for adsorption on the surface of the nanoparticles. So, the most probable mechanism for adsorption of chromium on the surface of nanoparticles is electrostatic/attraction repulsion [59]. The adsorption was highest at pH 2.0 for Cr(VI) on both the nanoparticle specimens and therefore, pH 2.0 was chosen as the optimum pH for forthcoming experiments.

The adsorption of Cu(II) and Cd(II) was less at lower pH but increased with the increase in pH. This behavior may be due to the reason that: lower pH leads to an abundance of hydronium ions ( $\text{H}_3\text{O}^+$ ) in the solution that causes competition between hydronium ions and Cu(II) or Cd(II) ions (copper and cadmium ions are present as  $\text{Cu}^{2+}$ ,  $\text{Cu}(\text{OH})^+$ ,  $\text{Cd}^{2+}$  and  $\text{Cd}(\text{OH})^+$  at lower pH) for adsorption onto nanoparticles thereby lowering the overall adsorption efficiency of these metal ions at lower pH [60]. Similar kind of results were reported by Ianos et al [61] who synthesized iron oxide/carbon nanocomposite for the removal of acid blue 129 dyes from simulated wastewater. They found that the adsorption capacity of acid blue at pH = 2.3 was  $4 \text{ mg g}^{-1}$ .

On the other hand, at higher pH values, the functional groups present on the surface of the nanoparticles like carboxylic acid, hydroxyls, phenol are deprotonated thus creating negative sites on the nanoparticles. This leads to an electrostatic attraction between these negatively charged adsorption sites and positively charged  $\text{Cu}^{2+}$  and  $\text{Cd}^{2+}$  ions thus, increasing their adsorption [62]. Since the adsorption was highest at pH 6.0 for both  $\text{Cu}^{2+}$  and  $\text{Cd}^{2+}$ , it was chosen as the optimum pH for both these ions.

The point – zero charge pH ( $\text{pH}_{\text{pzc}}$ ) plays an important role while studying the effect of pH (Fig. 8d). At  $\text{pH} < \text{pH}_{\text{pzc}}$ , the surface of the nanoparticles is positively charged and at  $\text{pH} >$

$\text{pH}_{\text{pzc}}$ , the surface of the nanoparticles is negatively charged (Fig. 8 d) [64]. Because the  $\text{pH}_{\text{pzc}}$  values were found to be 5.2 and 7.04 respectively for  $\text{Fe}_3\text{O}_4$  and  $\text{Fe}_3\text{O}_4/\text{AC}$ , it can be stated that the surface of these nanoparticles was positively charged below  $\text{pH}_{\text{pzc}}$  5.2 and 7.04. This confirmed that the hydrogen chromate ions were adsorbed through electrostatic attraction and  $\text{Cu}^{2+}$  and  $\text{Cd}^{2+}$  were repelled due to electrostatic repulsion between the two. While the surface of the nanoparticles was negatively charged above  $\text{pH}_{\text{pzc}}$  5.2 and 7.04, this led to the electrostatic repulsion between the nanoparticles surface and chromate ions and electrostatic attraction between nanoparticles surface and  $\text{Cu}^{2+}$  and  $\text{Cd}^{2+}$  ions.

#### 4.2.2. Metal ion concentration dependent studies

The effect of initial metal ion concentration by  $\text{Fe}_3\text{O}_4$  and  $\text{Fe}_3\text{O}_4/\text{AC}$  at concentration varying from 10-500  $\text{mg L}^{-1}$  keeping all other process variables constant (see details in pH dependent studies) is depicted in Fig. 8 (e and f). The figures revealed that the metal removal by both the nanoparticles decreased as the metal ion concentration in the solution was increased from 10 to 500  $\text{mg L}^{-1}$  in the solution. The metal removal efficiency decreased from 74.7 – 20.8% for Cr(VI), 60.0 – 10.5% for Cu(II) and 27.4 - 0 for Cd(II) in case of  $\text{Fe}_3\text{O}_4$  and 98.9 – 31.7% for Cr(VI), 99.9 – 12.5% for Cu(II) and 99.9 – 8.1% for Cd(II) by  $\text{Fe}_3\text{O}_4/\text{AC}$ . Our results are in agreement with Kera et al [63] who fabricated magnetic polypyrrole (PPy)–polyaniline (PANI)/iron oxide ( $\text{Fe}_3\text{O}_4$ ) nanocomposite for the removal of Cr(VI). This nanocomposite was efficient in removing 99% of Cr(VI) from aqueous solution at pH 2.0, initial metal ion concentration of 100  $\text{mg L}^{-1}$  and a nanocomposite dose of 0.05 g.

However, overall adsorption capacity of all the three metal ions increased on both the nanoparticles with an increase in concentration. It increased from 0.4 – 5.2  $\text{mg g}^{-1}$  for Cr(VI), 0.3 – 2.6  $\text{mg g}^{-1}$  for Cu(II) but no adsorption capacity for Cd(II) in case of  $\text{Fe}_3\text{O}_4$  whereas a similar

trend was observed by Fe<sub>3</sub>O<sub>4</sub>/AC i.e. 0.5 – 8.0 mg g<sup>-1</sup> for Cr(VI), 0.5 – 3.0 mg/g for Cu(II) and 0.5 – 2.0 mg g<sup>-1</sup> for Cd(II). This could be explained on the basis that the ionic radii (0.95 Å) of Cd(II) was high among the three ions. Moreover, Fe<sub>3</sub>O<sub>4</sub> doesn't contain any of the functional groups present on Fe<sub>3</sub>O<sub>4</sub>/AC. Thus, Cd(II) couldn't have access to the pores of the adsorbent, so it couldn't be removed.

The decrease in removal efficiency with an increase in metal ion concentration may be due to the fact that as the concentration of metal ion increases, increasingly more surface sites are covered and hence at higher metal ion concentration, the adsorption capacity of the nanoparticles get exhausted due to non-availability of free binding sites thus, resulting in a decrease in the overall removal efficiency [64]. It is therefore evident that, at low concentration ranges, the percentage of adsorption is high because of the availability of more active sites on the surface of nanoparticles. The increase in adsorption capacity can be explained on the basis that, an increase in initial metal ion concentration led to an increase in diffusion of Cr(VI), Cu(II) and Cd(II) ions from the solution phase to the surface of the nanoparticles due to an increase in the driving force of the metal ions which lead to the collisions between metal ions and the nanoparticles surface thus, resulting in an increase in adsorption capacity [22].

#### 4.2.3. Contact time dependent studies

Next, the effect of contact time on the removal of Cr(VI), Cu(II) and Cd(II) removal by Fe<sub>3</sub>O<sub>4</sub> and Fe<sub>3</sub>O<sub>4</sub>/AC was investigated to determine the optimum time taken to attain the equilibrium (Fig. 8g and h). The adsorption experiments were carried out by varying the contact time between 2 to 240 min keeping all other process variables constant. Fig. 8g and h depicts that, removal percentage increased with an increase in the contact time. The equilibrium was

achieved within 60, 120 and 30 min for Cr(VI), Cu(II) and Cd(II) respectively with Fe<sub>3</sub>O<sub>4</sub>. The removal efficiency increased from 30.4 to 58.3% for Cr(VI), 17.7 to 26.4% for Cu(II) and 4.4 to 8.2% for Cd(II) by Fe<sub>3</sub>O<sub>4</sub> after which it became constant and further removal of these metal ions was not observed.

While in case of Fe<sub>3</sub>O<sub>4</sub>/AC, removal of Cr(VI) reached 95.5 % within 45 min from the start of the experiment after which it became constant with no further removal. Similarly, 85.5 % Cu(II) was removed within 90 min, whereas 96.5 % Cd(II) was removed within 120 min. In case of Cr(VI) and Cd(II) ions, high removal efficiencies were achieved at early stage of the experiment, as 89.4 and 74.5 % removal reached within first 2.0 min, after which there was gradual increase till equilibrium time. Despite the short equilibrium time, the experiments were run for 240 min, in order to ensure complete adsorption of ions from the solution. Similar kind of results were reported by Wannahari et al [23] who combined activated carbon generated from sugarcane bagasse with magnetic iron oxide nanoparticles for the removal of Cu(II) ions. They interpreted that 77% of Cu(II) was removed at pH 4.0 within 60 min at 50 °C and would solve the problem of waste disposal.

It was observed that, the rate of Cr(VI), Cu(II) and Cd(II) binding with Fe<sub>3</sub>O<sub>4</sub> and Fe<sub>3</sub>O<sub>4</sub>/AC was faster at initial stages, which slowed down with the progress of time and remained almost constant after an optimum period or attainment of equilibrium. This may be attributed to the quick uptake of ions onto the large surface area of nanoparticles with an increase in the contact time, but after equilibrium was achieved, the removal efficiency of the metal ions slowed down as the free surface of the nanoparticles decreased due to the increased coverage by the bound ions [65]. Overall, the trend for both the nanoparticles is same i.e. with the increase in contact time; there is an increase in adsorption percentage.

#### 4.2.4. Temperature dependent studies

The effect of temperature on the removal of metal ions by  $\text{Fe}_3\text{O}_4$  and  $\text{Fe}_3\text{O}_4/\text{AC}$  was studied by varying the temperature in the range of 288 to 328 K again keeping all other process variables constant. The results revealed that the adsorption of ions increased with an increase in temperature (Fig. 9). The adsorption efficiency increased from 42.7 to 72.3% for Cr(VI), 19 to 46.8% for Cu(II) and 3.3 to 24.4% for Cd(II) by  $\text{Fe}_3\text{O}_4$ . While, in case of  $\text{Fe}_3\text{O}_4/\text{AC}$ , the increase in adsorption efficiency was observed from 69.7 to 99.9% for Cr(VI), 58.2 to 99.8% for Cu(II) and 65.4 to 99.8% for Cd(II) respectively. Aigbe et al [66] reported that the polypyrrole iron oxide magnetic nanocomposite prepared by them was useful in removing Cr(VI) ions from wastewater. The authors found that the highest Cr(VI) removal was 99.2% at following process conditions: magnetic field = 18.99 mT, Cr(VI) concentration =  $50 \text{ mg L}^{-1}$ , pH = 2.0, contact time = 150 min and temperature = 25 °C.

The results indicated that the maximum removal percentage was recorded at 328 K thus suggesting that the adsorption process was endothermic in nature. This may be due to the fact that, increase in temperature leads to an increase in mobility of the ions which in turn increases the interaction between the ions and the nanoparticles surface [67]. Although highest removal percentage was obtained at 328 K but 298 K was chosen as the optimum temperature for all the experiments as this temperature is suitable for practical application under field conditions.

On the basis of the results obtained from section 4.2.1 to 4.2.4, a table (Table 4) has been prepared mentioning the conditions required for the highest removal efficiency of synthesized nanocomposites for removal of heavy metals Cr(VI), Cu(II) and Cd(II).

#### 4.2.5. Thermodynamic studies

Thermodynamic studies help in predicting whether the adsorption mechanism is physical or chemical in nature. The thermodynamic parameters viz. standard Gibb's free energy ( $\Delta G^\circ$ ), standard enthalpy ( $\Delta H^\circ$ ) and standard entropy ( $\Delta S^\circ$ ) for the removal of Cr(VI) Cu(II), Cd(II) by  $\text{Fe}_3\text{O}_4$  and  $\text{Fe}_3\text{O}_4/\text{AC}$  were calculated by applying following equations [68]:

$$\Delta G^\circ = -RT \ln K \quad (4)$$

$$\Delta H^\circ = \left[ \frac{RT_1T_2}{(T_2 - T_1)} \right] \ln \left( \frac{K_2}{K_1} \right) \quad (5)$$

$$\Delta S^\circ = \left( \frac{\Delta H^\circ - \Delta G^\circ}{T} \right) \quad (6)$$

$$K = \left( \frac{qe}{Ce} \right) \quad (7)$$

where R ( $8.314 \text{ Jmol}^{-1}\text{K}^{-1}$ ) is the universal gas constant, K is the equilibrium constant at temperature T, T is the absolute temperature ( $^\circ\text{K}$ ),  $C_e$  ( $\text{mg L}^{-1}$ ) is the equilibrium concentration and  $q_e$  is the amount of Cr(VI) Cu(II), Cd(II) adsorbed on the surface of  $\text{Fe}_3\text{O}_4$  and  $\text{Fe}_3\text{O}_4/\text{AC}$ . Table 5 and 6 gives the thermodynamic parameters for adsorption of Cr(VI) Cu(II), Cd(II) adsorbed on the surface of  $\text{Fe}_3\text{O}_4$  and  $\text{Fe}_3\text{O}_4/\text{AC}$  at different temperatures.

Table 5 and 6 reveals that the negative value of  $\Delta G^\circ$  signifies that the adsorption process is feasible and spontaneous in nature. This is in agreement with the results obtained from the Langmuir separation factor  $R_L$  where the  $R_L$  values were found between 0 and 1 i.e. ( $0 < R_L < 1$ ) and the Freundlich exponent n was also greater than 1. With the increase in temperature, the value of  $\Delta G^\circ$  decreased indicating that the increase in temperature was favorable for the adsorption process [69]. The positive value of  $\Delta H^\circ$  signifies that the adsorption process is endothermic and irreversible in nature. The positive value of  $\Delta S^\circ$  signifies that the adsorption

process is a combination of the two simple processes i.e. Gibb's free energy ( $\Delta G^\circ$ ) and standard enthalpy ( $\Delta H^\circ$ ). Moreover, the positive values of  $\Delta S^\circ$  also indicated that the adsorbent surface had the affinity for Cr(VI), Cu(II) and Cd(II) ions and the degrees of disorder and randomness was high at the solid solution interface [70].

#### 4.2.6. Adsorption Isotherms

Batch adsorption data was described using Langmuir, Freundlich and Redlich-Peterson models. Langmuir adsorption model assumes that an adsorbent contains fixed number of binding sites. All the binding sites have same affinity for the adsorbate. Each site adsorbs only one molecule thus, forming a single monolayer. The linear form of Langmuir model and its separation factor  $R_L$  is expressed in equation 8 and 9:

$$\frac{C_e}{q_e} = \frac{1}{Q_0 b} + \frac{C_e}{Q_0} \quad (8)$$

$$R_L = \frac{1}{1 + bC_i} \quad (9)$$

Where,  $Q_0$  ( $\text{mg g}^{-1}$ ) is the maximum Langmuir adsorption capacity and  $b$  ( $\text{L mg}^{-1}$ ) is the Langmuir constant related to free energy. The Langmuir constants  $Q_0$  and  $b$  were calculated from the slope and intercept of the Langmuir plot of  $C_e$  versus  $C_e/q_e$  (Table 4). The value of  $Q_0$  was highest for Cr(VI) by both the nanoparticles i.e.  $8.06 \text{ mg g}^{-1}$  for Cr(VI),  $3.2 \text{ mg g}^{-1}$  for Cu(II) and  $2.15 \text{ mg g}^{-1}$  for Cd(II) by  $\text{Fe}_3\text{O}_4/\text{AC}$  while it was  $5.5 \text{ mg g}^{-1}$  for Cr(VI),  $2.7 \text{ mg g}^{-1}$  for Cu(II) and  $0.09 \text{ mg g}^{-1}$  for Cd(II) by  $\text{Fe}_3\text{O}_4$ .  $R^2$  (Regression coefficient) values were very high, being almost unity for Cr(VI), Cu(II) and Cd(II) by  $\text{Fe}_3\text{O}_4/\text{AC}$  as compared to  $\text{Fe}_3\text{O}_4$  [0.9660 for Cr(VI), 0.8179 for Cu(II) and 0.7331 for Cd(II) (Table 8). The values of Langmuir  $R^2$  for Cd(II) by  $\text{Fe}_3\text{O}_4$ ; Cr(VI), Cu(II) and Cd(II) by  $\text{Fe}_3\text{O}_4/\text{AC}$  were higher than Freundlich model thus,

indicating that Langmuir model fitted the data in good congruence, thereby indicating monolayer adsorption. The tea waste biomass loaded with nano-Fe<sub>3</sub>O<sub>4</sub> particles (TW/Fe<sub>3</sub>O<sub>4</sub>) composite was synthesized by Fan et al [71] for the removal of Cr(VI) from aqueous solution. The maximum Langmuir adsorption capacity was found to be 62.1 mg g<sup>-1</sup> by the authors at pH 2.0, contact time 10 h and temperature 25 °C.

The Langmuir separation factor ( $R_L$ ) which is a dimensionless constant indicates whether the adsorption process is favorable or not.  $R_L$  was calculated for the nanoparticles under study using equation 5 where  $b$  (L mg<sup>-1</sup>) and  $C_i$  (mg L<sup>-1</sup>) have already been explained. The criterion for favorable adsorption was chosen on the basis of  $R_L$  values. If  $R_L$  values are greater than 1.0, adsorption is unfavorable, if  $R_L$  values are equal to 1.0, adsorption is linear, if  $R_L$  values are between 0 and 1, adsorption is favorable and if  $R_L$  values are equal to 0, adsorption is irreversible. For the present system, the  $R_L$  values were between 0 and 1 (0.01-0.919) for Cr(VI), Cu(II) and Cd(II) by both the nanoparticles indicating favorable adsorption process (Table 8).

Freundlich adsorption model assumes that adsorbents have a heterogeneous surface having sites with different adsorption potential. It also assumes that stronger binding sites are occupied first and the binding strength decreases with the increasing degree of occupation. The Freundlich adsorption model in its linear form is given in equation 10:

$$\log_{10} q_e = \log_{10} (K_f) + \left(\frac{1}{n}\right) \log_{10} (C_e) \quad (10)$$

where  $K_f$  (mg g<sup>-1</sup>) is the Freundlich constant indicating adsorption capacity,  $n$  (L mg<sup>-1</sup>) is the adsorption intensity that is the measure of the change in affinity of the adsorbate with the change in adsorption density. The Freundlich constants  $K_f$  and  $n$  were calculated from the slope and

intercept of the plot of  $C_e$  versus  $\log_{10} q_e$  (Table 7). When  $n=1$ , Freundlich isotherm becomes linear and indicates that all the sites on the nanoparticles have equal affinity for the adsorbate. The adsorption intensity,  $n>1$ , indicates that affinity decreases with the increase in adsorption density and  $n<1$  indicates poor adsorption. The adsorption intensity ( $n$ ) values were found to be greater than 1 for all the three metal ions under study by  $Fe_3O_4$  and  $Fe_3O_4/AC$  (Table 7). The values of ( $R^2$ ) in Freundlich model for Cr(VI) and Cu(II) by  $Fe_3O_4$  viz. 0.9774 and 0.9483 were higher as compared to Langmuir model thus, indicating that Freundlich model fitted the data well confirming multilayer adsorption.

The Redlich–Peterson isotherm given by Redlich and Peterson is a combination of Langmuir and Freundlich isotherms. The numerator is from Langmuir isotherm and denominator has both Langmuir and Freundlich forms. This model includes three parameters into an empirical equation. Therefore, it can be applied to both homogenous and heterogeneous systems. This model does not follow ideal monolayer adsorption. The Redlich–Peterson model in its linear form is expressed in equation 11 [72]:

$$\ln\left(\frac{K_{RP}C_e - 1}{q_e}\right) = \ln(\alpha_{RP}) + \beta \ln(C_e) \quad (11)$$

where  $K_{RP}$  ( $L\ g^{-1}$ ) and  $\alpha_{RP}$  ( $L\ mg^{-1}$ ) are the Redlich–Peterson constants and  $\beta$  is the exponent which lies between 0 and 1.  $C_e$  ( $mg\ L^{-1}$ ) and  $q_e$  ( $mg/g$ ) are same as mentioned in Eq. (2) and (3) respectively in the Langmuir model. When exponent  $\beta$  approaches zero, equation 7 converts to Henry's law equation i.e. R–P equation approaches to Freundlich model at high concentration and when exponent  $\beta$  approaches one, equation 9 converts to Langmuir form. The value of  $\beta$  lied between 0 and 1 indicating favorable adsorption (Table 7).

#### 4.2.7. Adsorption Kinetics

The rate of reaction and reaction pathways are described by adsorption kinetics which depends upon the physical and chemical characteristics of the adsorbent. The adsorption kinetics was described using three models viz. pseudo-first order, pseudo-second order and intraparticle diffusion model. The adsorption in solid–liquid system was described by Pseudo-first-order kinetic model (Lagergren’s equation, equation 12). This model assumes that one metal ion is sorbed onto one sorption site on the surface of the adsorbent:

$$\log_{10} (q_e - q_t) = \log_{10} q_e - \frac{k_1}{2.303} t \quad (12)$$

where  $q_e$  is the adsorption capacity at equilibrium time and  $q_t$  ( $\text{mg g}^{-1}$ ) is the adsorption capacity at time  $t$  (min), and  $K_1$  ( $\text{min}^{-1}$ ) is the equilibrium rate constant for pseudo-first-order model. The value of  $K_1$  is derived from the slope of the linear plots of  $\log (q_e - q_t)$  versus time (min). The values of  $q_e$  (experimental) ( $\text{mg g}^{-1}$ ),  $q_e$  (calculated) ( $\text{mg g}^{-1}$ ),  $K_1$  ( $\text{min}^{-1}$ ) and  $R^2$  for Cr(VI), Cu(II) and Cd(II) by both the nanosorbents are given in Table 9. The table indicates that the values of regression coefficient ( $R^2$ ) for pseudo-first order model are poor and the calculated  $q_e$  values are not near to experimental  $q_e$  values thus, indicating a poor fit of this model to our data. Therefore, the adsorption of Cr(VI), Cu(II) and Cd(II) by  $\text{Fe}_3\text{O}_4$  and  $\text{Fe}_3\text{O}_4/\text{AC}$  was examined using pseudo-second-order model.

The pseudo-second-order model (equation 13) assumes that, one metal ion is sorbed onto two sorption sites on the surface of the adsorbent. This model has been used for analyzing chemisorption kinetics from liquid solutions.  $K_2$  ( $\text{g mg}^{-1} \text{min}^{-1}$ ) is the equilibrium rate constant and  $K_2q_e$  is the initial adsorption rate ( $\text{mg g}^{-1} \text{min}^{-1}$ ) for pseudo-second-order model. The values

of  $1/K_2q_e^2$  and  $1/q_e$  are derived from the intercept and slope of the linear plots of  $t/q_t$  versus time (min), which leads to calculation of the values of  $K_2$  and  $q_e$  (calculated):

$$\frac{t}{q_t} = \frac{1}{k_2q_e^2} + \frac{1}{q_e}t \quad (13)$$

The values of  $q_e$  (experimental) ( $\text{mg g}^{-1}$ ),  $q_e$  (calculated) ( $\text{mg g}^{-1}$ ),  $K_2$  ( $\text{g mg}^{-1} \text{min}^{-1}$ ) and  $R^2$  for Cr(VI), Cu(II) and Cd(II) by  $\text{Fe}_3\text{O}_4$  and  $\text{Fe}_3\text{O}_4/\text{AC}$  are given in Table 9. The table indicates that the values of regression coefficient are near to unity for Cr(VI), Cu(II) and Cd(II) by both the nanosorbents and values of  $q_e$  (experimental) and  $q_e$  (calculated) are almost near to each other thus, revealing that pseudo-second-order model fits the data well as compared to pseudo-first-order model.

Weber-Morris model (1963) is employed to further analyze the adsorption kinetics and to assess the importance of diffusion during the adsorption process. This model (equation 14) describes the movement of ions from bulk solution to the solid phase. It assumes that the adsorption process occurs in two steps. The first straight portion depicts macropore diffusion (i.e. diffusion of heavy metals from the solution to the exterior surface of the nanosorbent, which can be regarded as the external diffusion) and the second one represents micropore diffusion (i.e. diffusion from the surface of the nanosorbent into the pores):

$$q_t = K_{id}t^{0.5} + BL \quad (14)$$

where  $q_t$  is same as above,  $K_{id}$  is the intra-particle diffusion rate constant ( $\text{mg g}^{-1} \text{min}^{-1/2}$ ) which can be obtained from the slope of the straight line (slope of the plots between  $q_t$  and  $t^{1/2}$ ) and  $BL$  is the thickness of the boundary layer obtained from the intercept of the plots between  $q_t$  and time (min). The values of  $K_{id}$  and  $BL$  are given in Table 9. Larger the value of  $BL$ , greater is the

boundary layer effect. If intra-particle diffusion occurs, then  $q_t$  against  $t^{1/2}$  will be linear and the line will pass through the origin. But, in our case, the line didn't pass through the origin that means some other process is also involved in the adsorption. The intra-particle diffusion rate constants calculated from this model are not zero which indicates that the adsorption process may not be controlled by intra-particle diffusion model [73].

#### 4.2.8. Desorption studies

The regeneration and reuse of adsorbents has become economically important because of the high cost incurred in wastewater purification systems. Thus, it becomes necessary to check the reusability of the adsorbent for successive sorption-desorption cycles. For desorption experiments, Cr, Cu and Cd-loaded nanoparticles were first washed three times with deionized water in order to remove any loosely attached metal ion from their surface. They were then dried in hot air oven at 80 °C for 2h. Desorption was done using 0.1 M HCl (volume of desorbing agent = 10 mL) for 60 min in 15 mL disposable, capped tubes at  $26 \pm 1$  °C and agitation speed of 180 rpm on a rotary shaker. Hydrochloric acid is commonly used for eluting metal ions from adsorbents because of its frequent use in industry, relatively low cost and solubility of metal ions in it [74]. The nanoparticles were separated by a strong magnet and the supernatant was collected for measuring of metal concentration in the solution. Residual concentration of metal ions in the solution was determined in a similar way as in the adsorption experiments. The reusability of the nanoparticles was tested by following the above adsorption–desorption process up to four cycles for Cr(VI), Cu(II) and Cd(II) ions (Fig. 10). The metal recovery was calculated by the following equation 15:

$$\% \text{ Desorption Efficiency} = \frac{\text{Amount of metal ion desorbed}}{\text{Amount of metal ion sorbed}} \times 100 \quad (15)$$

Fig. 10 depicted that desorption efficiency decreased with each sorption-desorption cycle. Desorption efficiency of Cu(II) and Cd(II) was found to be fairly high for first cycle i.e 80.6% and 83.9% respectively but quiet low for Cr(VI) i.e. 21.3% by Fe<sub>3</sub>O<sub>4</sub>/AC which reduced gradually with the proceeding cycles.

While, the desorption efficiency was high for Cu(II) and Cd(II), it was substantially low for Cr(VI). This may be due to the reason that Cr(VI) might be chemically bonded with the Fe<sub>3</sub>O<sub>4</sub>/AC thus, restricting its desorption. It was found that 0.1 M HCl was quite effective in desorbing Cr(VI), Cu(II) and Cd(II) ions from the surface of nanosorbents. The obtained results verified that the Fe<sub>3</sub>O<sub>4</sub> nanoparticles synthesized with co-precipitation process can be recovered effectively for the re-adsorption of the metal ions. The regeneration of Fe<sub>3</sub>O<sub>4</sub>/AC also indicated that adsorption of Cr(VI), Cu(II) and Cd(II) on to the Fe<sub>3</sub>O<sub>4</sub>/AC was a reversible process and the nanoparticles were quiet stable even after four adsorption-desorption cycles.

#### **4.2.9 Comparison of adsorption capacity with other adsorbents**

The maximum adsorption capacity of Fe<sub>3</sub>O<sub>4</sub>/AC nanocomposite for the removal of Cr(VI), Cu(II) and Cd(II) was compared with other adsorbents reported in the literature and the values are given in Table 10. It is clear from Table 10, that the adsorption capacity of Fe<sub>3</sub>O<sub>4</sub>/AC nanocomposite is comparable with other nanomaterials suggesting that, it is effective in removing Cr(VI), Cu(II) and Cd(II) from aqueous solutions [75-83, 62, 84-85].

## **5. Conclusion**

In this article, the adsorption potential of Fe<sub>3</sub>O<sub>4</sub> and Fe<sub>3</sub>O<sub>4</sub>/AC nanoparticles was investigated for the removal of Cr(VI), Cu(II) and Cd(II) ions. TEM analysis revealed that the

synthesized nanoparticles were spherical in nature with an average particle size of 12.9 nm for Fe<sub>3</sub>O<sub>4</sub> and 12.3 nm for Fe<sub>3</sub>O<sub>4</sub>/AC. The XRD analysis of Fe<sub>3</sub>O<sub>4</sub> and Fe<sub>3</sub>O<sub>4</sub>/AC confirmed the presence of magnetite phase exhibiting average crystal size similar to that indicated by the TEM analysis. The maximum magnetic strength was found to be 59.3 and 52.2 Am<sup>2</sup> kg<sup>-1</sup> respectively of Fe<sub>3</sub>O<sub>4</sub> and Fe<sub>3</sub>O<sub>4</sub>/AC. The optimum adsorption pH was found to be 2.0 for Cr(VI) and 6.0 for Cu(II) and Cd(II) respectively. The removal efficiency of nanoparticles decreased with an increase in the concentration i.e. 74.7 – 20.8% for Cr(VI), 60.0 – 10.5% for Cu(II) and 27.4 - 0 for Cd(II) by Fe<sub>3</sub>O<sub>4</sub> and 98.9 – 31.7% for Cr(VI), 99.9 – 12.5% for Cu(II) and 99.9 – 8.1% for Cd(II) by Fe<sub>3</sub>O<sub>4</sub>/AC. The adsorption efficiency for Cr(VI) and Cd(II) was high in the beginning of the experiments as indicated by 89.4 and 74.5% removal in the first 2.0 min. The conditions for the highest removal efficiency of synthesized nanocomposite for the removal of Cr(VI), Cu(II) and Cd(II) were pH = 2.0 and 6.0, temperature = 25±1 ° C, initial metal ion concentration = 50 mg L<sup>-1</sup> contact time = 60 and 45 min for Cr(VI) by Fe<sub>3</sub>O<sub>4</sub> and Fe<sub>3</sub>O<sub>4</sub>/AC, 120 and 90 min for Cu(II) and Cd(II) by Fe<sub>3</sub>O<sub>4</sub> and Fe<sub>3</sub>O<sub>4</sub>/AC. The maximum Langmuir adsorption capacity was 8.06 mg g<sup>-1</sup> for Cr(VI), 3.2 mg g<sup>-1</sup> for Cu(II) and 2.15 mg g<sup>-1</sup> for Cd(II) by Fe<sub>3</sub>O<sub>4</sub>/AC while it was 5.5 mg g<sup>-1</sup> for Cr(VI), 2.7 mg g<sup>-1</sup> for Cu(II) and 0.09 mg g<sup>-1</sup> for Cd(II) by Fe<sub>3</sub>O<sub>4</sub>. The desorption efficiency was fairly high in first cycle i.e. 80 and 83% for Cu(II) and Cd(II) which decreased gradually till the fourth cycle. In case of Cr(VI), substantially lower desorption efficiency of 23.2 % was determined.

### **Acknowledgement**

The authors would like to thank Laboratory of Green Chemistry for providing all the facilities for carrying out this work. Dr. Hua Jiang, Aalto University for TEM analysis, Mr. Simo

for SEM/EDS, MAMK, Ms. Laura Lukkarinen for TGA analysis, MAMK and Sanjana Gunasee, University of Mauritius, for her assistance in analyzing the TGA results.

## References

- [1] H. Sharififard, M. Nabavinia, M. Soleimani, Evaluation of adsorption efficiency of activated carbon/chitosan composite for removal of Cr(VI) and Cd(II) from single and bi-solute dilute solution, *Adv. Environ. Technol.* 4 (2016) 215-227.
- [2] V.K. Gupta, A. Nayak, Cadmium removal and recovery from aqueous solutions by novel adsorbents prepared from orange peel and Fe<sub>2</sub>O<sub>3</sub> nanoparticles, *Chem. Eng. J.* 180 (2012) 81-90.
- [3] T.A. Saleh, V.K. Gupta, Column with CNT/magnesium oxide composite for lead (II) removal from water, *Environ. Sci. Pollut. Res.* 19 (2012) 1224-1228.
- [4] W. Shotyk, G.L. Roux, A. Sigel, H. Sigel, R.K.O. Sigel, *Metal ions in biological systems*; Taylor and Francis: Boca Raton 43 (2005) Chapter 10.
- [5] World Health Organization. *World health statistics 2010*. World health organization (2010).
- [6] M.A.A. Zaini, R. Okayama, M. Machida, Adsorption of aqueous metal ions on cattle-manure compost based activated carbons, *J. Hazard. Mater.* 170 (2009) 1119-1124.
- [7] J. Barnhart, Occurrences, uses, and properties of chromium, *Regulatory Toxicology and Pharmacology*, 26 (1997) S3-S7.
- [8] M.E. Losi, C. Amrhein, W.T. Frankenberger Jr, *Environmental biochemistry of chromium*, In reviews of environmental contamination and toxicology, Springer New York (1994) 91-121.
- [9] K. Mohanty, M. Jha, B.C. Meikap, M.N. Biswas, Removal of chromium (VI) from dilute aqueous solutions by activated carbon developed from Terminalia Arjuna nuts activated with zinc chloride, *Chem. Eng. Sci.* 60 (2005) 3049-3059.

- [10] L. Levankumar, V. Muthukumar, M.B. Gobinath, Batch adsorption and kinetics of chromium (VI) removal from aqueous solutions by *Ocimum americanum* L. seed pods, *J. Hazard. Mater.* 161 (2009) 709-713.
- [11] M. Bilal, J.A. Shah, T. Ashfaq, S.M.H. Gardazi, A.A. Tahir, A. Pervez, H. Haroon, Q. Mahmood, Waste biomass adsorbents for copper removal from industrial wastewater – A review, *J. Hazard. Mater.* 263 (2013) 322–333.
- [12] X.J. Hu, Y.G. Liu, H. Wang, A.W. Chen, G.M. Zeng, S.M. Liu, Y.M. Guo, X. Hu, T.T. Li, Y.Q. Wang, L. Zhou, S.H. Liu, Removal of Cu(II) ions from aqueous solution using sulfonated magnetic graphene oxide composite, *Sep. Purif. Technol.* 108 (2013) 189–195.
- [13] S. Lan, X. Wu, L. Li, M. Li, F. Guo, S. Gan, Synthesis and characterization of hyaluronic acid-supported magnetic microspheres for copper ions removal, *Colloids Surf. A: Physicochem. Eng. Asp.* 425 (2013) 42–50.
- [14] L.C.A. Oliveira, R.V.R.A. Rios, J.D. Fabris, V. Garg, K. Sapag, R.M. Lago, Solid waste from leather industry as adsorbent of organic dyes in aqueous-medium, *Carbon* 40 (2002) 2177–2183.
- [15] H.L. Zhang, X.C. Li, G.H. He, J.J. Zhan, D. Liu, Preparation of magnetic composite hollow microsphere and its adsorption capacity for basic dyes, *Ind. Eng. Chem. Res.* 52 (2013) 16902–16910.
- [16] D.L. Tran, V.H. Le, H.L. Pham, T.M.N. Hoang, T.Q. Nguyen, T.T. Luong, P.T. Ha, X.P. Nguyen, Biomedical and environmental applications of magnetic nanoparticles, *Adv. Nat. Sci. Nanosci. Nanotechnol.* 1 (2010) 045013.
- [17] N. Ilankoon, Use of iron oxide magnetic nanosorbents for Cr(VI) removal from aqueous solutions: A review, *Int. J. Eng. Res. Appl.* 4 (2014) 55-63.

- [18] P.N. Dave, L.V. Chopda, Application of iron oxide nanomaterials for the removal of heavy metals, *J. Nanotechnol.* 398569(2014)14.
- [19] N. Ghasemi, M. Ghasemi, S. Moazeni, P. Ghasemi, N.S. Alharbi, V.K. Gupta, S. Agarwal, I.V. Burakova, A.G. Tkachev, Zn(II) removal by amino-functionalized magnetic nanoparticles: Kinetics, isotherm, and thermodynamic aspects of adsorption, *J. Ind. Eng. Chem.* 62 (2018) 302–310.
- [20] M.O. Ojemaye, O.O. Okoh, A.I. Okoh, Surface modified magnetic nanoparticles as efficient adsorbents for heavy metal removal from wastewater: Progress and prospects, *Mater. Express* 7 (2017) 439-456.
- [21] C. Sanchez, H. Arribart, M.M.G. Guille, Biomimetism and bioinspiration as tools for the design of innovative materials and systems, *Nature Mater.* 4 (2005) 277- 288.
- [22] M. Xu, Y. Zhang, Z. Zhang, Y. Shen, M. Zhao, G. Pan, Study on the adsorption of  $\text{Ca}^{2+}$ ,  $\text{Cd}^{2+}$  and  $\text{Pb}^{2+}$  by magnetic  $\text{Fe}_3\text{O}_4$  yeast treated with EDTA dianhydride, *Chem. Eng. J.* 168 (2011) 737-745.
- [23] R. Wannahari, P. Sannasi, M.F.M. Nordin, H. Mukhtar, Sugarcane bagasse derived nano magnetic adsorbent composite (SCB-NMAC) for removal of  $\text{Cu}^{2+}$  from aqueous solution, *ARPN J. Eng. Appl. Sci.* 13 (2018) 1-9.
- [24] Y.F. Shen, J. Tang, Z.H. Nie, Y.D. Wang, Y. Ren, L. Zuo, Tailoring size and structural distortion of  $\text{Fe}_3\text{O}_4$  nanoparticles for the purification of contaminated water, *Bioresour. Technol.* 100 (2009) 4139-4146.
- [25] B. Kakavandi, R.R. Kalantary, M. Farzadkia, A.H. Mahvi, A. Esrafil, A. Azari, A.R. Yari, A.B. Javid, Enhanced chromium (VI) removal using activated carbon modified by zero valent iron and silver bimetallic nanoparticles, *J. Environ. Health Sci. Eng.* 12 (2014) 115.

- [26] D. Gholamvaisi, S. Azizian, M. Cheraghi, Preparation of magnetic-activated carbon nanocomposite and its application for dye removal from aqueous solution, *J. Dispersion Sci. Technol.* 35 (2014) 1264–1269.
- [27] A.C. Affam, C.C. Wong, M.A.B. Seyam, C.A.A.F. Matt, J.L.A. Sumbai, A.M. Evuti, Preparation, characterization and adsorption study of granular activated carbon/iron oxide composite for the removal of boron and organics from wastewater, *E3S Web Conf.* 34 (2018) 02006.
- [28] S. Yao, S. Sun, S. Wang, Z. Shi, Adsorptive removal of lead ion from aqueous solution by activated carbon/iron oxide magnetic composite, *Indian J. Chem. Technol.* 23 (2016) 146-152.
- [29] S.Z. Liang, L.F. Mei, Y.S. Hua, Adsorptive removal of phosphate from aqueous solutions using activated carbon loaded with Fe(III) oxide, *New Carbon Mater.* 26 (2011) 299–306.
- [30] C.S. Castro, M.C. Guerreiro, M. Goncalves, L.C.A. Oliveira, A.S. Anastácio, Activated carbon/iron oxide composites for the removal of atrazine from aqueous medium, *J. Hazard Mater.* 164 (2009) 609–614.
- [31] L.C.A. Oliveira, R.V.R.A. Rios, J.D. Fabris, V. Garg, K. Sapag, R.M. Lago, Activated carbon/iron oxide magnetic composites for the adsorption of contaminants in water, *Carbon* 40 (2002) 2177–2183.
- [32] E.K. Faulconer, N.V. Hoogesteijn von Reitzenstein, D.W. Mazyck, Optimization of magnetic powdered activated carbon for aqueous Hg(II) removal and magnetic recovery, *J. Hazard. Mater.* 199-200 (2012) 9-14.
- [33] K.A. Tan, N. Morad, T.T. Teng, I. Norli, P. Panneerselvam, Removal of cationic dye by magnetic nanoparticle ( $\text{Fe}_3\text{O}_4$ ) impregnated onto activated maize cob powder and kinetic study of dye waste adsorption, *APCBEE Procedia* 1 (2012) 83-89.

- [34] D. Mohan, A. Sarswat, V.K. Singh, M. Alexandre-Franco, C.U. Pittam Jr., Development of magnetic activated carbon from almond shell for trinitrophenol removal from water, *Chem. Eng. J.* 172 (2011) 1111-1125.
- [35] M. Jain, V.K. Garg, K. Kadirvelu, Chromium removal from aqueous system and industrial wastewater by agricultural wastes, *Bioremediation J.* 17 (2013) 30–39.
- [36] G. Sun, X. Xu, Sunflower stalks as adsorbents for color removal from textile wastewater, *Ind. Eng. Chem. Res.* 36 (1997) 808–812.
- [37] H. Benaissa, M.A. Elouchdi, Removal of copper ions from aqueous solutions by dried sunflower leaves. *Chem. Eng. Process. Process Intensificat.* 46 (2007) 614-622.
- [38] N. Thinakaran, P. Baskaralingam, M. Pulikesi, P. Panneerselvam, S. Sivanesan, Removal of acid violet 17 from aqueous solutions by adsorption onto activated 499 carbon prepared from sunflower seed hull, *J. Hazard. Mater.* 151 (2008) 316–322.
- [39] L.M. Soldatkina, E.V. Sagaidak, V.V. Menchuk, Adsorption of cationic dyes from aqueous solutions on sunflower husk. *J. Water Chem. Technol.* 31 (2009) 238–243.
- [40] B.I. Hussein, Removal of copper ions from wastewater by adsorption with modified and unmodified sunflower stalks, *J. Eng.* 16 (2010) 5411-5421.
- [41] K.Y. Foo, B.H. Hameed, Preparation and characterization of activated carbon from sunflower seed oil residue via microwave assisted  $K_2CO_3$  activation, *Bioresour. Technol.* 102, (2011) 9794-9799.
- [42] A. Witek-Krowiak, Analysis of temperature-dependent biosorption of  $Cu^{2+}$  ions on sunflower hulls: Kinetics, equilibrium and mechanism of the process, *Chem. Eng. J.* 192 (2012) 13–20.

- [43] Z. Zou, Y. Tang, C. Jiang, J. Zhang, Efficient adsorption of Cr(VI) on sunflower seed hull derived porous carbon, *J. Environ Chem Eng.* 3 (2015) 898-905.
- [44] M. Feizi, M. Jalali, Removal of heavy metals from aqueous solutions using sunflower, potato, canola and walnut shell residues, *J. Taiwan Inst. Chem. Eng.* 54 (2016) 125-136.
- [45] S. Srisorrachatr, Modified sunflower seed husks for metal ions removal from wastewater, *Chem Eng Trans.* 57 (2017) 247-252.
- [46] S. Karagoz, T. Tay, S. Ucar, M. Erdem, Activated carbons from waste biomass by sulfuric acid activation and their use on methylene blue adsorption, *Bioresour. Technol.* 99 (2008) 6214–6222.
- [47] B. Sivakumar, C. Kannan, S. Karthikeyan, Preparation and characterization of activated carbon prepared from *Balsamorhiza hirsuta* wood waste through various activation processes, *Rasayan J. Chem.* 5 (2012) 321-327.
- [48] M. Jain, V.K. Garg, K. Kadirvelu, Adsorption of hexavalent chromium from aqueous medium onto carbonaceous nanosorbents prepared from sunflower biomass, *Environ. Manage.* 91 (2010) 949-957.
- [49] P. Lodeiro, J.L. Barriada, R. Herrero, M.E. Sastre de Vicente, The marine macroalga *Cystoseira baccata* as biosorbent for Cd(II) and Pb(II) removal: kinetic and equilibrium studies, *Environ. Pollut.* 142 (2006) 264-273.
- [50] V.K. Gupta, I. Tyagi, H. Sadegh, R.S. Ghoshekandi, A.S.H. Makhlof, B. Maazinejad, Nanoparticles as adsorbent; A positive approach for removal of noxious metal ions: A review, *Sci. Technol. Dev.* 34 (2015) 195-214.

- [51] X. Hu, H. Wang, Y. Liu, Statistical analysis of main and interaction effects on Cu(II) and Cr(VI) decontamination by nitrogen-doped magnetic graphene oxide, *Sci. Rep.* 34378 (2016)1-11.
- [52] D.J. Dunlop, Ö. Özdemir, *Rock Magnetism: fundamentals and frontiers*, Cambridge (Cambridge University Press), Cambridge, (2001)596.
- [53] X. Lu, J. Jiang, K. Sun, X. Xie, Preparation and characterization of sisal fiber-based activated carbon by chemical activation with zinc chloride, *Bull. Korean Chem. Soc.* 35 (2014) 103.
- [54] A.A. Zabaniotou, E.K. Kantarelis, D.C. Theodoropoulos, Sunflower shells utilization for energetic purposes in an integrated approach of energy crops: Laboratory study pyrolysis and kinetics, *Bioresour. Technol.* 99 (2008) 3174-3181.
- [55] D. Ferdous, A.K. Dalai, S.K. Bej, R.W. Thring, Pyrolysis of lignins: experimental and kinetics studies. *Energ. Fuel* 16 (2002) 1405–1412.
- [56] G. Wang, W. Li, B. Li, H. Chen, TG study on pyrolysis of biomass and its three components under syngas, *Fuel* 87 (2008) 552–558
- [57] X. Yao, K. Xu, Y. Liang, Comparing the thermo-physical properties of rice husk and rice straw as feedstock for thermochemical conversion and characterization of their waste ashes from combustion, *BioResources*, 11 (2016) 10549-10564.
- [58] D. Mohan, C.U. Pittman Jr., Activated carbons and low cost nanosorbents for remediation of tri and hexavalent chromium from water – Review, *J. Hazard. Mater.* B137 (2006) 762–811.
- [59] M. Jain, V.K. Garg, K. Kadirvelu, Equilibrium and kinetic studies for sequestration of Cr(VI) from simulated wastewater using sunflower waste biomass, *J. Hazar. Mater.* 171 (2009) 328-334.

- [60] M.M.A. El-Latif, A.M. Ibrahim, M.S. Showman, R.R.A. Hamide, Alumina/Iron Oxide nanocomposite for cadmium ions removal from aqueous solutions, *Int. J. Nonferrous Metallur.* 2 (2013) 47-62.
- [61] R. Ianos, C. Pacurariu, S.G. Muntean, E. Muntean, M.A. Nistor, D. Niznanský, Combustion synthesis of iron oxide/carbon nanocomposites, efficient adsorbents for anionic and cationic dyes removal from wastewaters, *J. Alloys Compd.* 741 (2018) 1235-1246.
- [62] D. Mohan, H. Kumar, A. Saraswat, M. Alexandro-Franco, C.U. Pittam Jr., Cadmium and lead remediation using magnetic oak wood and oak bark fast pyrolysis biochars, *Chem. Eng. J.* 236 (2014) 513-528.
- [63] N.H. Kera, M. Bhaumik, K. Pillay, S.S. Ray, A. Maity, Selective removal of toxic Cr(VI) from aqueous solution by adsorption combined with reduction at a magnetic nanocomposite surface, *J. Colloid Interf. Sci.* 503 (2017) 214–228.
- [64] H. Guo, S. Zhang, Z. Kou, S. Zhai, W. Ma, Y. Yang, Removal of cadmium(II) from aqueous solutions by chemically modified maize straw, *Carbohydr. Polym.* 115 (2015) 177-185.
- [65] Z. Rafiq, R. Nazir, D.E. Shahwar, M.R. Shah, S. Ali, Utilization of magnesium and zinc oxide nano-adsorbents as potential materials for treatment of copper electroplating industry wastewater, *Environ. Chem. Eng.* 2 (2014) 642-651.
- [66] U.O. Aigbe, R. Das, W.H. Ho, V. Srinivasu, A. Maity, A novel method for removal of Cr(VI) using polypyrrole magnetic nanocomposite in the presence of unsteady magnetic fields, *Sep. Purif. Technol.* 194 (2018) 377–387.
- [67] N.N. Nassar, Rapid removal and recovery of Pb(II) from wastewater by magnetic nanoadsorbents, *J. Hazard. Mater.* 184 (2010) 538–546.

- [68] M.I. Panayotova, Kinetics and thermodynamics of copper ions removal from wastewater by use of zeolite. *Waste Manage.* 21 (2001) 671–676.
- [69] L. Xu, X. Zheng, H. Cui, Z. Zhu, J. Liang, J. Zhou, Equilibrium, kinetic, and thermodynamic studies on the adsorption of cadmium from aqueous solution by modified biomass ash, *Bioinorganic Chemistry Applications*. 3695604 (2017) 1-9.
- [70] M.E. Saleh, A.A. El-Refaey, A.H. Mahmoud, Effectiveness of sunflower seed husk biochar for removing copper ions from wastewater: a comparative study, *Soil Water Res.* 11 (2016) 53–63.
- [71] S. Fan, Y. Wang, Y. Li, J. Tang, Z. Wang, J. Tang, X. Li, K Hu. Facile synthesis of tea waste/Fe<sub>3</sub>O<sub>4</sub> nanoparticle composite for hexavalent chromium removal from aqueous solution, *RSC Adv.* 7 (2017) 7576 -7590.
- [72] O. Redlich, D.L. Peterson, A useful adsorption isotherm, *J. Phys. Chem.* 63 (1959) 1024.
- [73] Y. Liu, M. Chen, Y.M Hao, Study on the adsorption of Cu(II) by EDTA functionalized Fe<sub>3</sub>O<sub>4</sub> magnetic nanoparticles, *Chem. Eng. J.* 218 (2013) 46-54.
- [74] G. M. Naja, B. Volesky, *Treatment of Metal-Bearing Effluents: Removal and Recovery. Handbook on Heavy Metals in the Environment.* Taylor & Francis and CRC Press, Boca Raton, FL, Chapter 9, 247-291(2010)
- [75] F. Ge, M.M. Li, H. Ye, B.X. Zhao, Effective removal of heavy metal ions Cd<sup>2+</sup>, Zn<sup>2+</sup>, Pb<sup>2+</sup>, Cu<sup>2+</sup> from aqueous solution by polymer-modified magnetic nanoparticles, *J. Hazard. Mater.* 211–212 (2012) 366–372.
- [76] A.Z.M. Badruddoza, Z.B.Z. Shawon, T.W.J. Daniel, K. Hidajat, M.S. Uddin, Fe<sub>3</sub>O<sub>4</sub>/cyclodextrin polymer nanocomposites for selective heavy metals removal from industrial wastewater, *Carbohydr. Polym.* 91 (2013) 322–332.

- [77] N.N. Nassar, Kinetics, equilibrium and thermodynamic studies on the adsorptive removal of nickel, cadmium and cobalt from wastewater by superparamagnetic iron oxide nano-adsorbents, *The Canadian J. Chem. Eng.* 9999 (2011) 1–8.
- [78] S.S. Banerjee, D.H. Chen, Fast removal of copper ions by gum arabic modified magnetic nano-adsorbent, *J. Hazard. Mater.* 147 (2007) 792–799.
- [79] Y.J. Tu, C.F. You, C.K. Chang, Kinetics and thermodynamics of adsorption for Cd on green manufactured nano-particles. *J. Hazard. Mater.* 235–236 (2012) 116–122.
- [80] N. Kataria, V.K. Garg, Green synthesis of Fe<sub>3</sub>O<sub>4</sub> nanoparticles loaded sawdust carbon for cadmium(II) removal from water: Regeneration and mechanism, 208(2018) 818-828.
- [81] Y. Li, S. Zhu, Q. Liu, Z. Chen, J. Gu, C. Zhu, T. Lu, D. Zhang, J. Mac, N-doped porous carbon with magnetic particles formed in situ for enhanced Cr(VI) removal, *Water Res.* 47 (2013) 4188-4197.
- [82] S.H. Huang, D.H. Chen, Rapid removal of heavy metal cations and anions from aqueous solutions by an amino-functionalized magnetic nano-adsorbent, *J. Hazard. Mater.* 163 (2009) 174–179.
- [83] S. Nethaji, A. Sivasamy, A.B. Mandal Preparation and characterization of corn cob activated carbon coated with nano-sized magnetite particles for the removal of Cr(VI), *Bioresour. Technol.* 134 (2013) 94–100.
- [84] H. Li, Z. Li, T. Liu, X. Xiao, Z. Peng, L. Deng, A novel technology for biosorption and recovery hexavalent chromium in wastewater by bio-functional magnetic beads. *Bioresour. Technol.* 99 (2008) 6271–6279.

[85] G. López- Téllez, C.E. Barrera-Díaz, P. Balderas-Hernández, G. Roa-Morales, B. Bilyeu, Removal of hexavalent chromium in aquatic solutions by iron nanoparticles embedded in orange peel pith, Chem. Eng. J. 173 (2011) 480-485.

**Fig. 1.** <sup>P</sup>FT-IR spectra of Fe<sub>3</sub>O<sub>4</sub>, Cd, Cu and Cr loaded Fe<sub>3</sub>O<sub>4</sub> & Fe<sub>3</sub>O<sub>4</sub>/AC and Cr, Cu, Cd loaded Fe<sub>3</sub>O<sub>4</sub>/AC and AC, <sup>Q</sup>Powder XRD of Fe<sub>3</sub>O<sub>4</sub> and Fe<sub>3</sub>O<sub>4</sub>/AC

**Fig. 2.** SEM micrographs of (a) Fe<sub>3</sub>O<sub>4</sub> (b) Cr loaded Fe<sub>3</sub>O<sub>4</sub> (c) Cu loaded Fe<sub>3</sub>O<sub>4</sub> (d) Cd loaded Fe<sub>3</sub>O<sub>4</sub> (e) Fe<sub>3</sub>O<sub>4</sub>/AC (f) Cr loaded Fe<sub>3</sub>O<sub>4</sub>/AC (g) Cu loaded Fe<sub>3</sub>O<sub>4</sub>/AC and (h) Cd loaded Fe<sub>3</sub>O<sub>4</sub>/AC

**Fig. 3.** EDS spectra of (a) Fe<sub>3</sub>O<sub>4</sub> (b) Cr loaded Fe<sub>3</sub>O<sub>4</sub> (c) Cu loaded Fe<sub>3</sub>O<sub>4</sub> (d) Cd loaded Fe<sub>3</sub>O<sub>4</sub> (e) Fe<sub>3</sub>O<sub>4</sub>/AC (f) Cr loaded Fe<sub>3</sub>O<sub>4</sub>/AC (g) Cu loaded Fe<sub>3</sub>O<sub>4</sub>/AC and (h) Cd loaded Fe<sub>3</sub>O<sub>4</sub>/AC and in the inset, elemental composition of Fe<sub>3</sub>O<sub>4</sub>, metal loaded Fe<sub>3</sub>O<sub>4</sub> and Fe<sub>3</sub>O<sub>4</sub>/AC, metal loaded Fe<sub>3</sub>O<sub>4</sub>/AC.

**Fig. 4.** TEM images of (a) Fe<sub>3</sub>O<sub>4</sub> (b) Fe<sub>3</sub>O<sub>4</sub>/AC (c) Particle size distribution of Fe<sub>3</sub>O<sub>4</sub> (d) Particle size distribution of Fe<sub>3</sub>O<sub>4</sub>/AC and in the inset, selected area diffraction pattern of Fe<sub>3</sub>O<sub>4</sub> and Fe<sub>3</sub>O<sub>4</sub>/AC.

**Fig. 5.** SEM images of Activated Carbon

**Fig. 6.** Magnetic moment loop of Fe<sub>3</sub>O<sub>4</sub> and Fe<sub>3</sub>O<sub>4</sub>/AC

**Fig. 7.** TGA/DTG profile of Fe<sub>3</sub>O<sub>4</sub> and Fe<sub>3</sub>O<sub>4</sub>/AC

**Fig. 8.** <sup>a,b,c,d</sup>Effect of pH on Cr(VI), Cu(II) and Cd(II) removal by Fe<sub>3</sub>O<sub>4</sub>, Fe<sub>3</sub>O<sub>4</sub>/AC, without nanoparticles and pH<sub>pzc</sub>, <sup>e,f</sup>Effect of initial metal ion concentration on Cr(VI), Cu(II) and Cd(II) removal by Fe<sub>3</sub>O<sub>4</sub> and Fe<sub>3</sub>O<sub>4</sub>/AC, <sup>g,h</sup>Effect of contact time on Cr(VI), Cu(II) and Cd(II) removal by Fe<sub>3</sub>O<sub>4</sub> and Fe<sub>3</sub>O<sub>4</sub>/AC

**Fig. 9.** Effect of temperature on Cr(VI), Cu(II) and Cd(II) removal by Fe<sub>3</sub>O<sub>4</sub> and Fe<sub>3</sub>O<sub>4</sub>/AC

**Fig.10.** Desorption of Cr(VI), Cu(II) and Cd(II) from Fe<sub>3</sub>O<sub>4</sub>/AC by HCl

**Table 1.** Surface area, pore volume and average pore diameter of Sunflower Head Waste, Fe<sub>3</sub>O<sub>4</sub> and Fe<sub>3</sub>O<sub>4</sub>/AC.

Material	Surface Area (m <sup>2</sup> /g)	Pore Volume cm <sup>3</sup> g <sup>-1</sup>	Average Pore Diameter (Å°)
Sunflower Head Waste	0.99	0.0007	3.037
Fe <sub>3</sub> O <sub>4</sub>	47.87	0.0355	3.245
Fe <sub>3</sub> O <sub>4</sub> /AC	51.1	0.0386	3.293

**Table 2.** Average crystal sizes of Fe<sub>3</sub>O<sub>4</sub> phases.

Nanoparticles	Fe <sub>3</sub> O <sub>4</sub> (220) nm	Fe <sub>3</sub> O <sub>4</sub> (311) nm	Fe <sub>3</sub> O <sub>4</sub> (400) nm	Fe <sub>3</sub> O <sub>4</sub> (511) nm
Fe <sub>3</sub> O <sub>4</sub>	16	17	21	15
Fe <sub>3</sub> O <sub>4</sub> /AC	16	17	21	16

**Table 3.** Magnetic properties of Fe<sub>3</sub>O<sub>4</sub> and Fe<sub>3</sub>O<sub>4</sub>/AC.

Nanoparticles	Coercivity [Hc (mT)]	Saturation magnetization [Js (Am <sup>2</sup> /Kg)]	Remanence (Am <sup>2</sup> /Kg)
Fe <sub>3</sub> O <sub>4</sub>	5.2	59.3	5.3
Fe <sub>3</sub> O <sub>4</sub> /AC	3.6	52.2	3.9

**Table 4.** Conditions for highest removal efficiency of synthesized nanocomposite for the removal of Cr(VI), Cu(II) and Cd(II).

Heavy Metals	pH	Temperature	Initial concentration	Contact time	
				Fe <sub>3</sub> O <sub>4</sub>	Fe <sub>3</sub> O <sub>4</sub> /AC

Cr(VI)	2.0	25±1 °C	50 mg L <sup>-1</sup>	60 min	45 min
Cu(II)	6.0	25±1 °C	50 mg L <sup>-1</sup>	120 min	90 min
Cd(II)	6.0	25±1 °C	50 mg L <sup>-1</sup>	120 min	90 min

**Table 5.** Thermodynamic parameters for adsorption of Cr(VI), Cu(II), Cd(II) by Fe<sub>3</sub>O<sub>4</sub> at different temperatures.

Thermodynamic parameters for adsorption of Cr(VI) onto Fe <sub>3</sub> O <sub>4</sub>			
Temp (K)	$\Delta G^\circ$ (J mol <sup>-1</sup> )	$\Delta H^\circ$ (J mol <sup>-1</sup> )	$\Delta S^\circ$ (J mol <sup>-1</sup> K <sup>-1</sup> )
288	7875.3	44602.6	127.5
298	6602.0	16011.6	31.6
308	6286.3	19598.4	43.2
318	5854.0	15427.3	30.1
328	5553.0	0	-16.9
Thermodynamic parameters for adsorption of Cu(II) onto Fe <sub>3</sub> O <sub>4</sub>			
Temp (K)	$\Delta G^\circ$ (J mol <sup>-1</sup> )	$\Delta H^\circ$ (J mol <sup>-1</sup> )	$\Delta S^\circ$ (J mol <sup>-1</sup> K <sup>-1</sup> )
288	11026.4	49458.9	133.4
298	9692.3	0	-32.5
308	10017.5	33017.3	74.7
318	9269.3	24947.3	49.3
328	8775.5	0	-26.8
Thermodynamic parameters for adsorption of Cd(II) onto Fe <sub>3</sub> O <sub>4</sub>			
Temp (K)	$\Delta G^\circ$ (J mol <sup>-1</sup> )	$\Delta H^\circ$ (J mol <sup>-1</sup> )	$\Delta S^\circ$ (J mol <sup>-1</sup> K <sup>-1</sup> )
288	15260.7	69459.6	188.2
298	13341.6	28060.8	49.4
308	12871.7	41345.9	92.4
318	11965.3	43814.8	100.2
328	10965.3	0	-33.4

**Table 6.** Thermodynamic parameters for adsorption of Cr(VI), Cu(II), Cd(II) by Fe<sub>3</sub>O<sub>4</sub>/AC at different temperatures.

Thermodynamic parameters for adsorption of Cr(VI) onto Fe <sub>3</sub> O <sub>4</sub> /AC			
Temp (K)	$\Delta G^\circ$ (J mol <sup>-1</sup> )	$\Delta H^\circ$ (J mol <sup>-1</sup> )	$\Delta S^\circ$ (J mol <sup>-1</sup> K <sup>-1</sup> )
288	5178.4	154838.3	519.7
298	-239.3	49906.2	168.3
308	-1710.1	67994.6	226.3
318	-3973.9	208731.1	668.9
328	-10665.3	0	32.5
Thermodynamic parameters for adsorption of Cu(II) onto Fe <sub>3</sub> O <sub>4</sub> /AC			

Temp (K)	$\Delta G^\circ$ (J mol <sup>-1</sup> )	$\Delta H^\circ$ (J mol <sup>-1</sup> )	$\Delta S^\circ$ (J mol <sup>-1</sup> K <sup>-1</sup> )
288	6378.8	103820.2	338.3
298	3005.3	87908.2	284.9
308	130.6	58548.6	189.7
318	-1765.6	221045.1	700.7
328	-8772.2	0.0	26.7

Thermodynamic parameters for adsorption of Cd(II) onto Fe<sub>3</sub>O<sub>4</sub>/AC

Temp (K)	$\Delta G^\circ$ (J mol <sup>-1</sup> )	$\Delta H^\circ$ (J mol <sup>-1</sup> )	$\Delta S^\circ$ (J mol <sup>-1</sup> K <sup>-1</sup> )
288	5648.5	185092.5	623.1
298	-582.2	67762.6	229.3
308	-2873.9	17100.4	64.9
318	-3524.3	223473.2	713.8
328	-10665.3	0.0	32.5

**Table 7.** Langmuir, Freundlich and Redlich- Peterson isotherm parameters for the removal of Cr(VI), Cu(II) and Cd(II) by Fe<sub>3</sub>O<sub>4</sub> and Fe<sub>3</sub>O<sub>4</sub>/AC.

	Langmuir Parameters					
	Fe <sub>3</sub> O <sub>4</sub>			Fe <sub>3</sub> O <sub>4</sub> /AC		
	Chromium	Copper	Cadmium	Chromium	Copper	Cadmium
$Q_o$ (mg g <sup>-1</sup> )	5.5	2.7	0.09	8.06	3.2	2.15
$b$ (L mg <sup>-1</sup> )	0.02	0.008	0.07	0.17	0.33	0.11
$R^2$	0.9660	0.8179	0.7331	0.9994	0.9998	0.9750
Freundlich Parameters						
$K_f$ (mg g <sup>-1</sup> )	0.29	0.16	0.03	1.44	1.4	1.4
$n$ (L mg <sup>-1</sup> )	1.9	2.4	1.71	2.7	6.7	7.1
$R^2$	0.9774	0.9483	0.5995	0.9336	0.9274	0.6194
Redlich- Peterson Parameters						
$K_{RP}$ (L/g)	1	2	1	0.5	2	4
$\alpha_{RP}$ (L/mg)	2.9	0.93	27.9	13.5	0.9290	0.99
$\beta$	0.52	0.93	0.06	0.07	0.9285	1.00
$R^2$	0.9814	0.9996	0.8442	0.5165	0.9996	0.9974

**Table 8.**  $R_L$  values for the removal of Cr(VI), Cu(II) and Cd(II) by Fe<sub>3</sub>O<sub>4</sub> and Fe<sub>3</sub>O<sub>4</sub>/AC.

I. Conc. (mg L <sup>-1</sup> )	$R_L$					
	Fe <sub>3</sub> O <sub>4</sub>			Fe <sub>3</sub> O <sub>4</sub> /AC		
	Chromium	Copper	Cadmium	Chromium	Copper	Cadmium
10	0.854	0.919	0.595	0.365	0.232	0.575
20	0.746	0.850	0.423	0.224	0.131	0.729
30	0.662	0.791	0.329	0.161	0.091	0.391

<b>40</b>	0.594	0.740	0.268	0.126	0.070	0.267
<b>50</b>	0.540	0.694	0.227	0.103	0.057	0.203
<b>75</b>	0.439	0.602	0.164	0.071	0.039	0.127
<b>100</b>	0.370	0.532	0.128	0.054	0.029	0.092
<b>150</b>	0.281	0.431	0.089	0.037	0.020	0.060
<b>200</b>	0.227	0.362	0.068	0.028	0.015	0.044
<b>300</b>	0.163	0.275	0.047	0.019	0.010	0.029
<b>500</b>	0.105	0.185	0.029	0.011	0.006	0.017

**Table 9.** Pseudo I<sup>st</sup>-order, Pseudo-II<sup>nd</sup>-order and Intraparticle Diffusion kinetic parameters for the removal of Cr(VI), Cu(II) and Cd(II) by Fe<sub>3</sub>O<sub>4</sub> and Fe<sub>3</sub>O<sub>4</sub>/AC.

	Pseudo-I <sup>st</sup> -order Kinetic parameters					
	Fe <sub>3</sub> O <sub>4</sub>			Fe <sub>3</sub> O <sub>4</sub> /AC		
	Chromium	Copper	Cadmium	Chromium	Copper	Cadmium
$q_e$ (exp) (mg g <sup>-1</sup> )	2.38	0.74	0.25	2.39	2.14	2.47
$q_e$ (cal) (mg g <sup>-1</sup> )	0.14	0.36	0.12	0.31	0.74	0.38
$K_1$ (min <sup>-1</sup> )	0.0987	0.0223	0.0119	0.106	0.047	0.02
$R^2$	0.5166	0.4238	0.4609	0.692	0.5481	0.6295
Pseudo-II <sup>nd</sup> -order Kinetic parameters						
$q_e$ (exp) (mg g <sup>-1</sup> )	2.38	0.74	0.25	2.39	2.14	2.47
$q_e$ (cal) (mg g <sup>-1</sup> )	2.37	0.75	0.25	2.39	2.16	2.47
$K_2$ (g mg <sup>-1</sup> min <sup>-1</sup> )	3.076	0.2387	0.669	2.21	0.23	0.28
$R^2$	1	0.9983	0.9947	1	0.9998	0.9998
Intraparticle Diffusion Parameters						
$K_{ID}$ (mg/g min)	0.0613	0.79	0.011	0.645	0.0792	0.0819
$BL$	1.7834	1.278	0.1125	1.7534	1.278	1.5831
$R^2$	0.1951	0.4312	0.6326	0.2172	0.4312	0.3472

**Table 10.** Comparison of adsorption capacity of Fe<sub>3</sub>O<sub>4</sub>/AC with other adsorbents.

Adsorbents	Adsorption Capacity (mg/g)	pH	Temp.	Heavy Metals			References
				Cr(VI)	Cu(II)	Cd(II)	
Fe <sub>3</sub> O <sub>4</sub> @APS@AA-co-CA MNPs	29.6	5.5	25 °C	-	-	-	[75]
Carboxymethyl Cyclodextrin (CM-CD) polymer modified Fe <sub>3</sub> O <sub>4</sub> nanoparticles	27.7	5.5	25 °C	-	-	-	[76]
Iron oxide nanoparticles	18.59	5.5	25 °C	-	-	-	[77]

Iron oxide nanoparticles	17.6	5.1	27 °C	-	Cu(II)	-	[78 ]
Magnetic nano-particles CuFe <sub>2</sub> O <sub>4</sub>	17.54	6.0	45 °C	-	-	Cd(II)	[79 ]
Fe <sub>3</sub> O <sub>4</sub> /SC	15	6.5	27 °C	-	-	Cd(II)	[80]
RHC-mag-CN	16	3.0	25 °C	Cr(VI)	-	-	[81]
Amino functionalized magnetic nanosorbent	12.43			-	Cu(II)	-	[82]
Amino functionalized magnetic nanosorbent	11.24			Cr(VI)	-	-	[82]
MCCAC	9.67	2.0	27 °C	Cr(VI)	-	-	[83]
Magnetic oak bark char	7.40	5.0	25 °C	-	-	Cd(II)	[62]
Biofunctional magnetic beads	6.73	1.0	28 °C	Cr(VI)	-	-	[84]
Iron oxide NPs embedded in orange peel pith	5.37	1.0	-	Cr(VI)	-	-	[85]
Magnetic oak wood char	2.87	5.0	25 °C	-	-	Cd(II)	[62 ]
Fe <sub>3</sub> O <sub>4</sub> /AC	4.4	2.0	25 °C	Cr(VI)	-	-	This study
Fe <sub>3</sub> O <sub>4</sub> /AC	2.7	6.0	25 °C	-	Cu(II)	-	This study
Fe <sub>3</sub> O <sub>4</sub> /AC	2.9	6.0	25 °C	-	-	Cd(II)	This study

Fig. 1

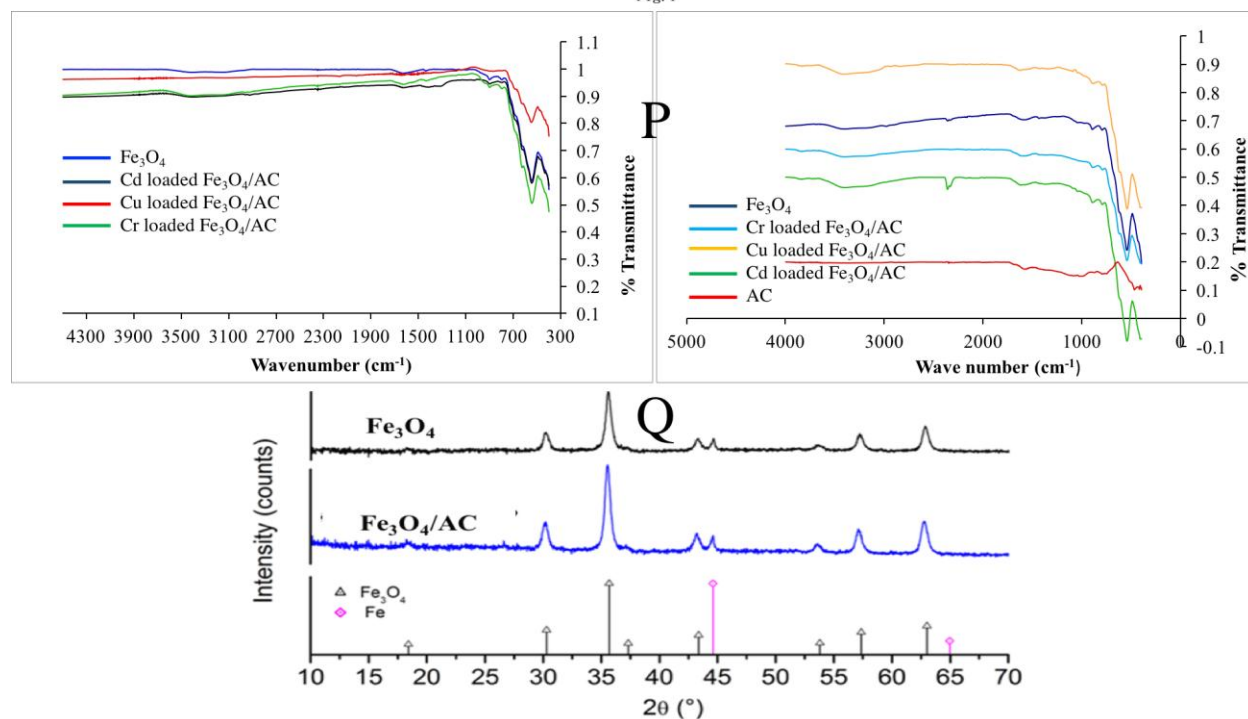


Fig. 2

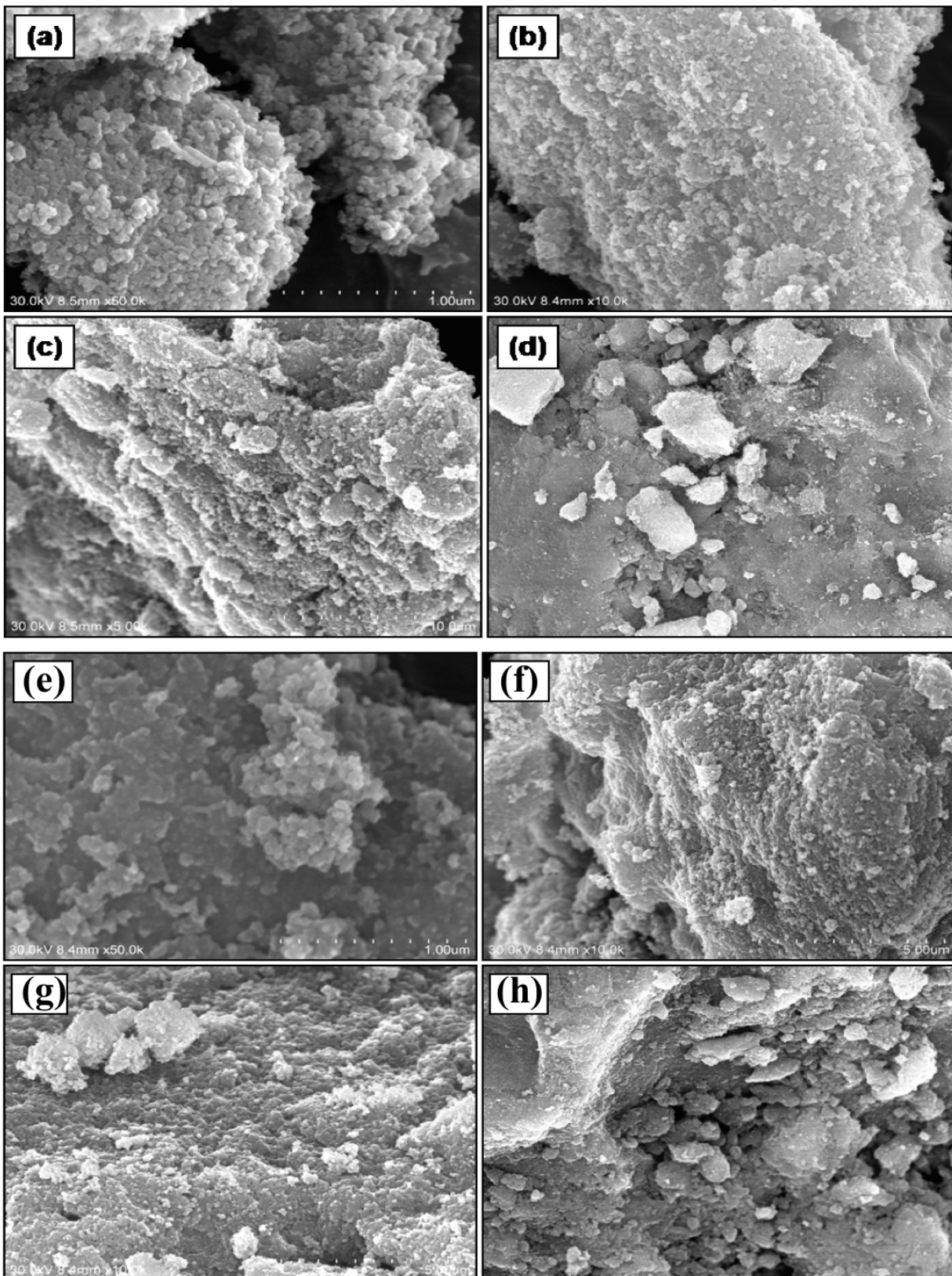


Fig.3

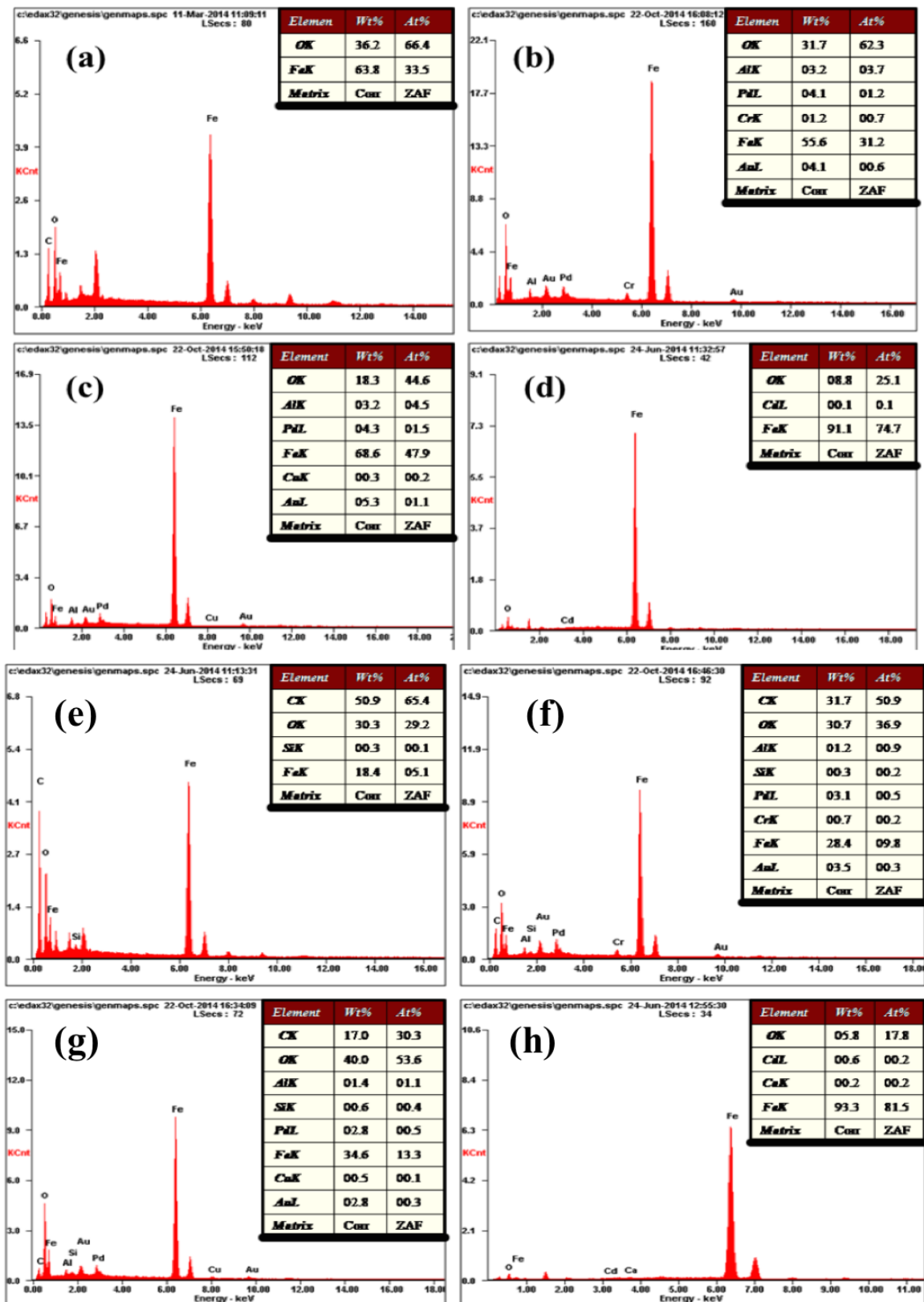


Fig.4

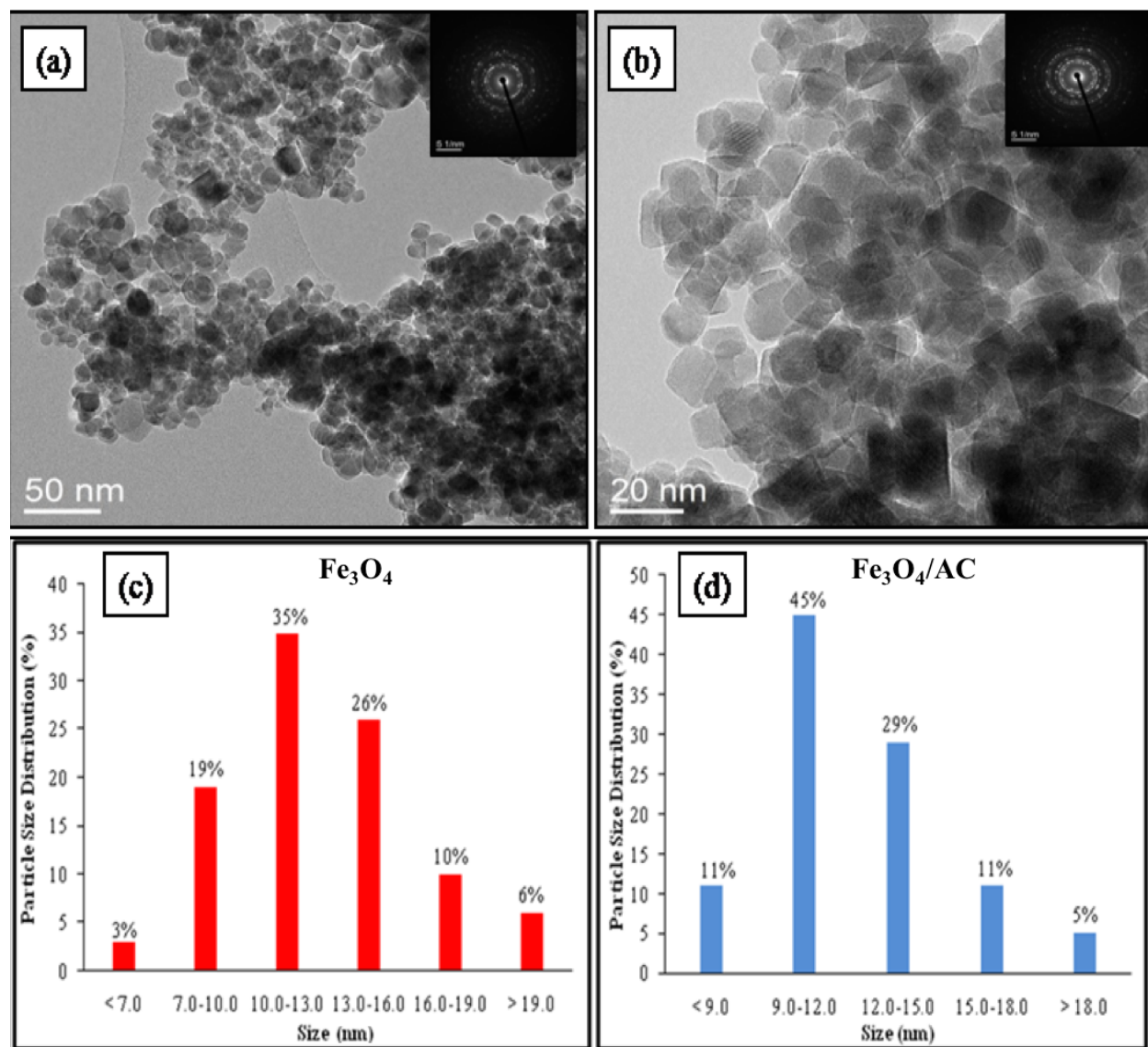


Fig.5

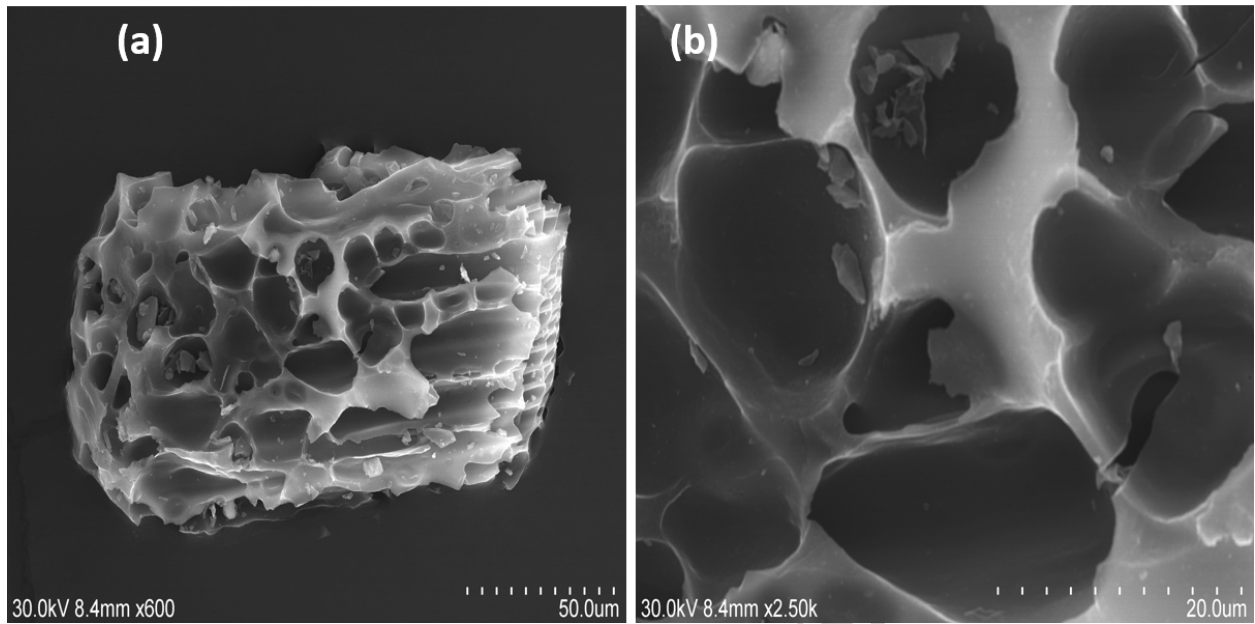


Fig.6

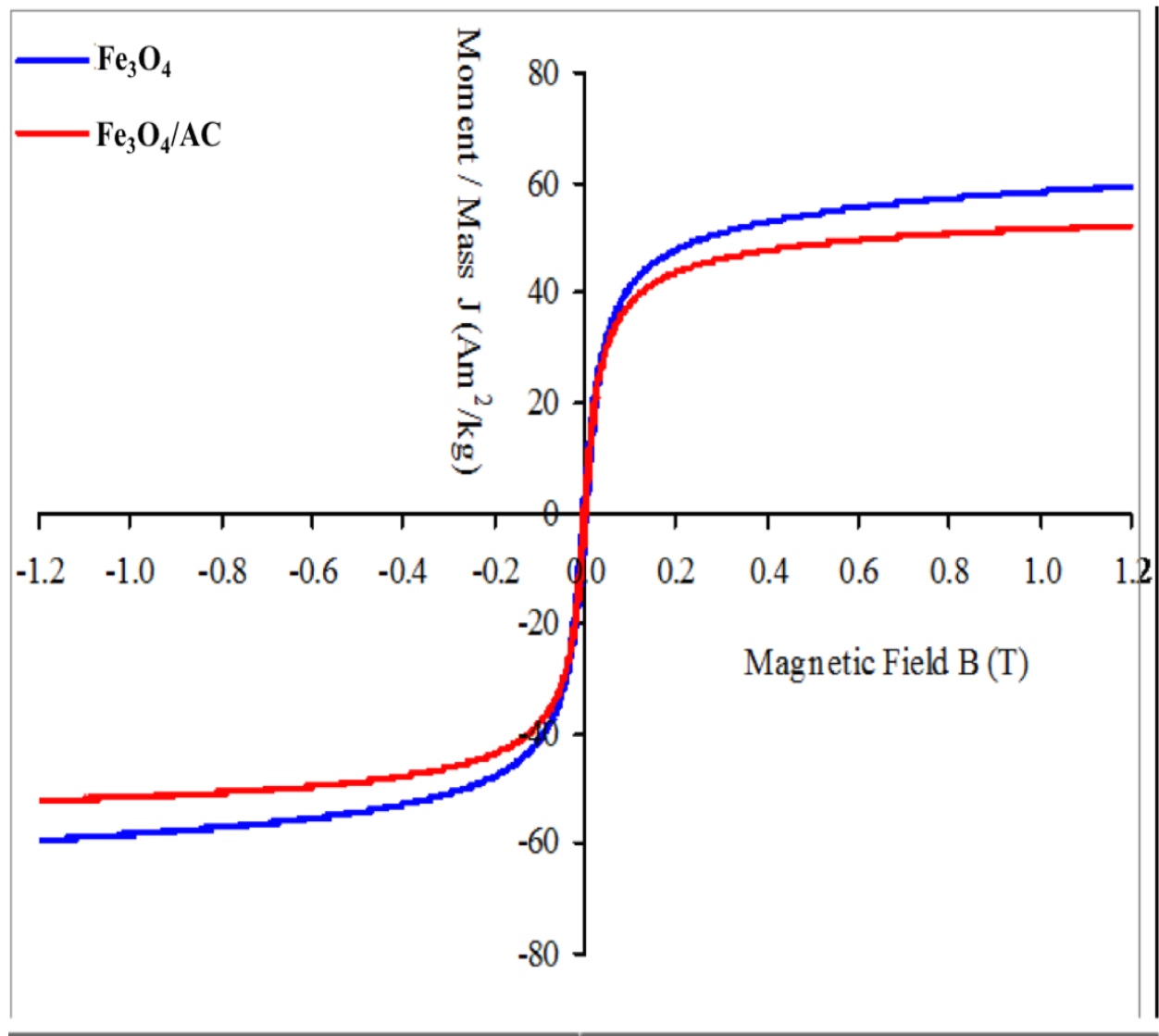


Fig.7

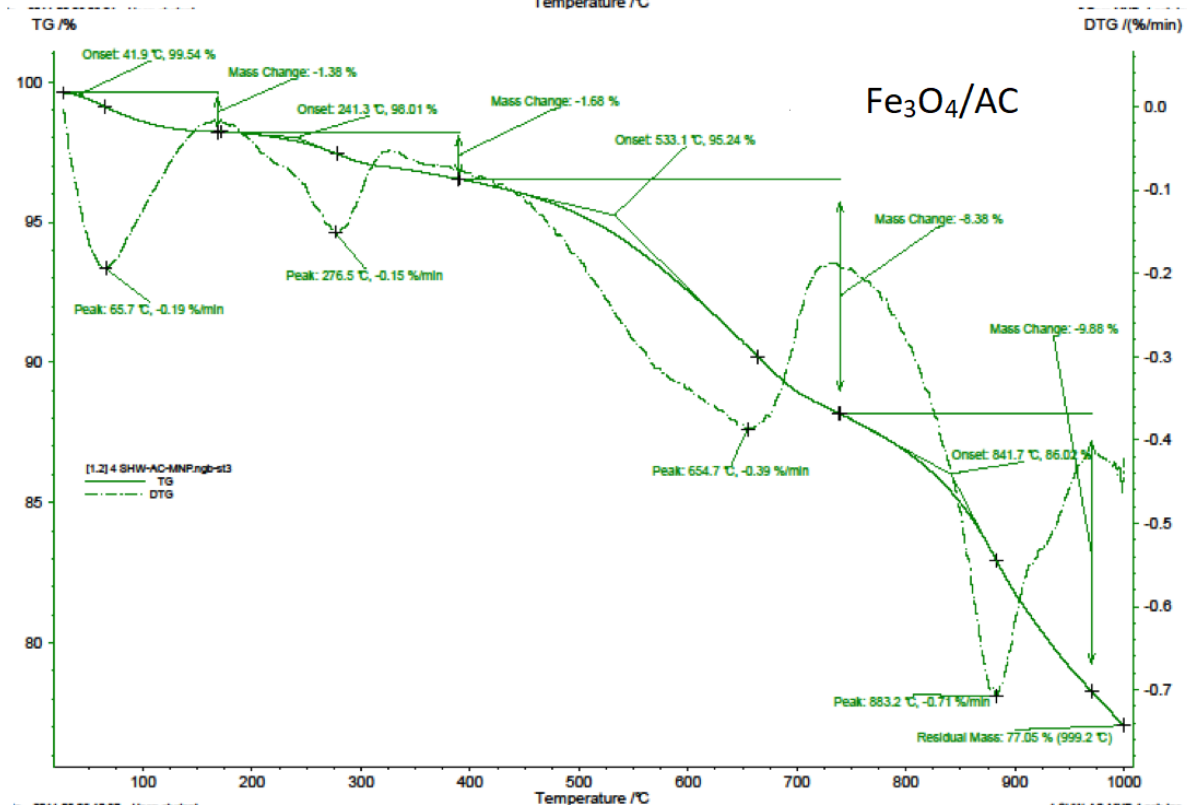
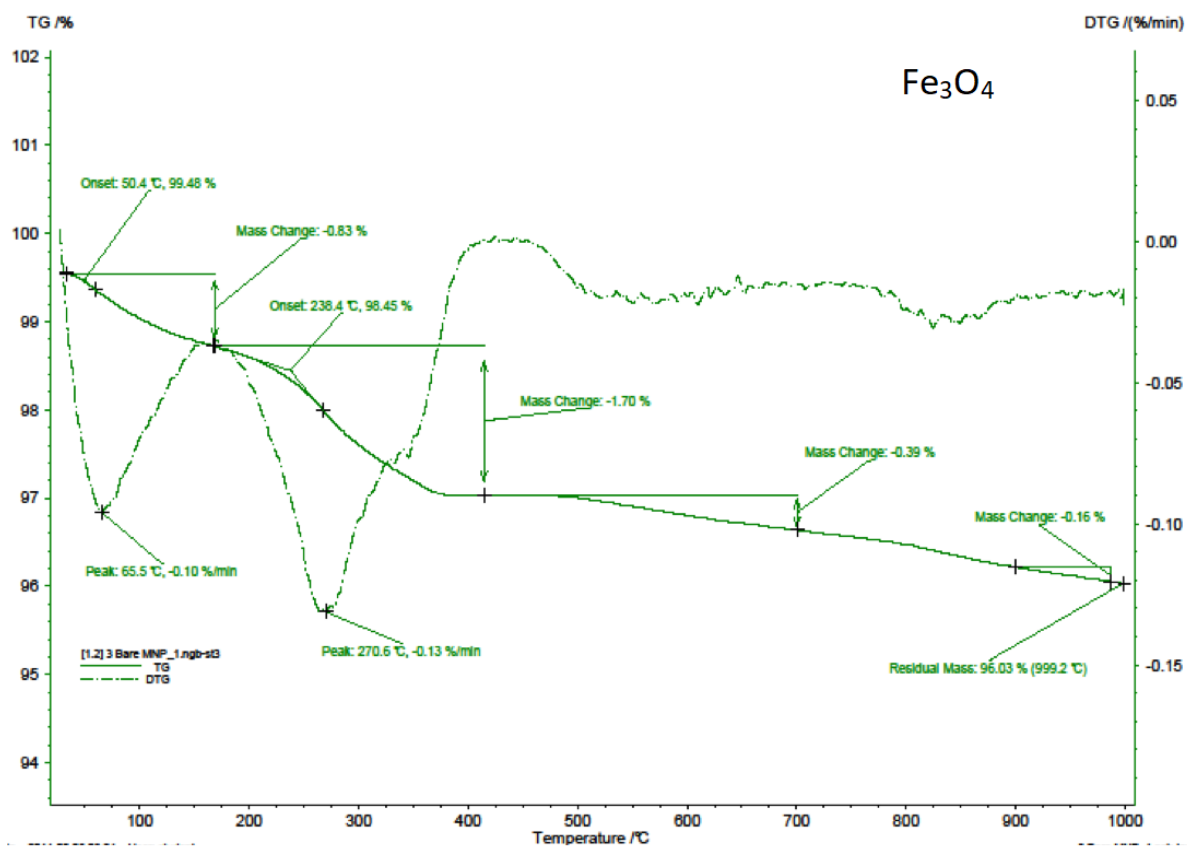


Fig.8

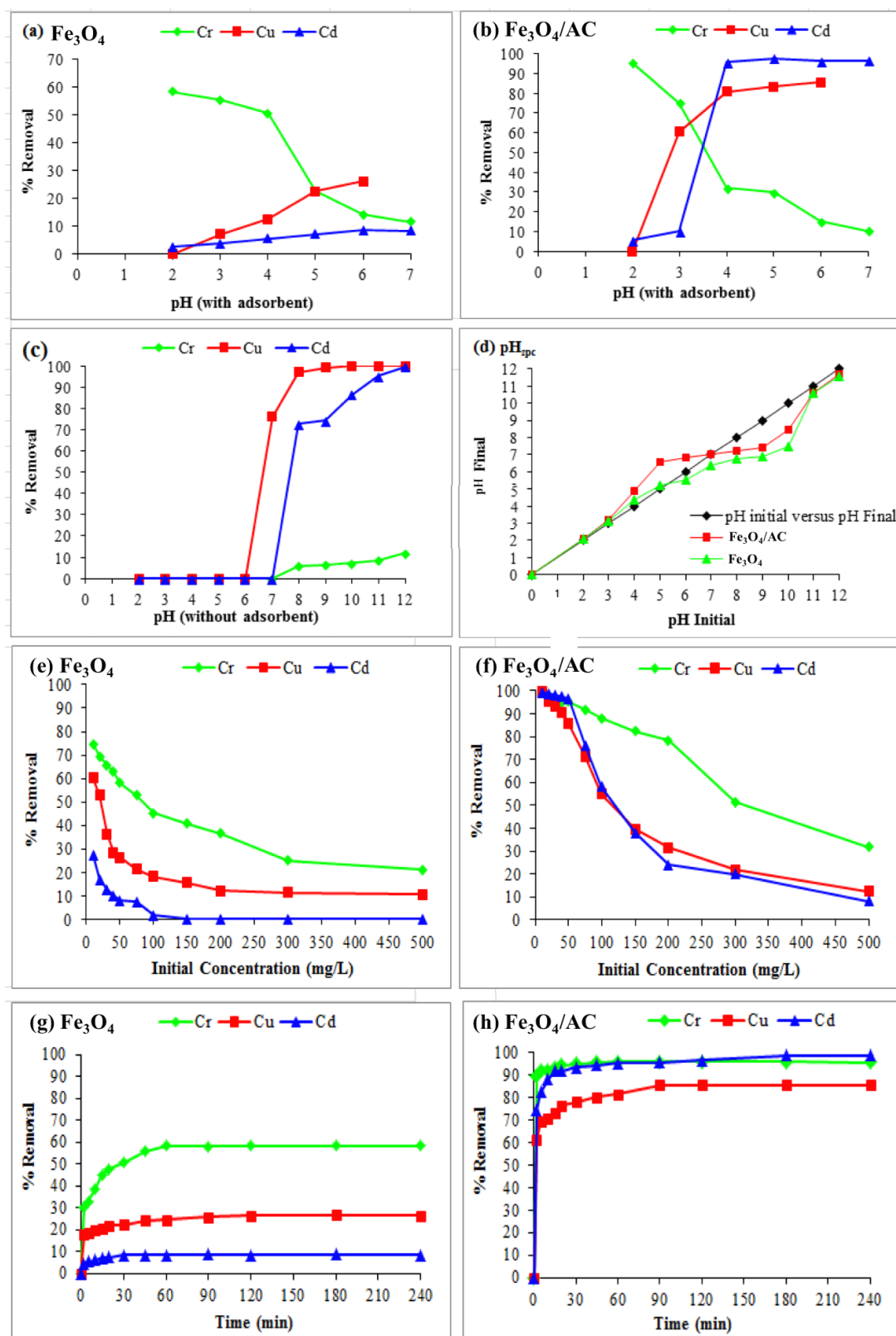


Fig.9

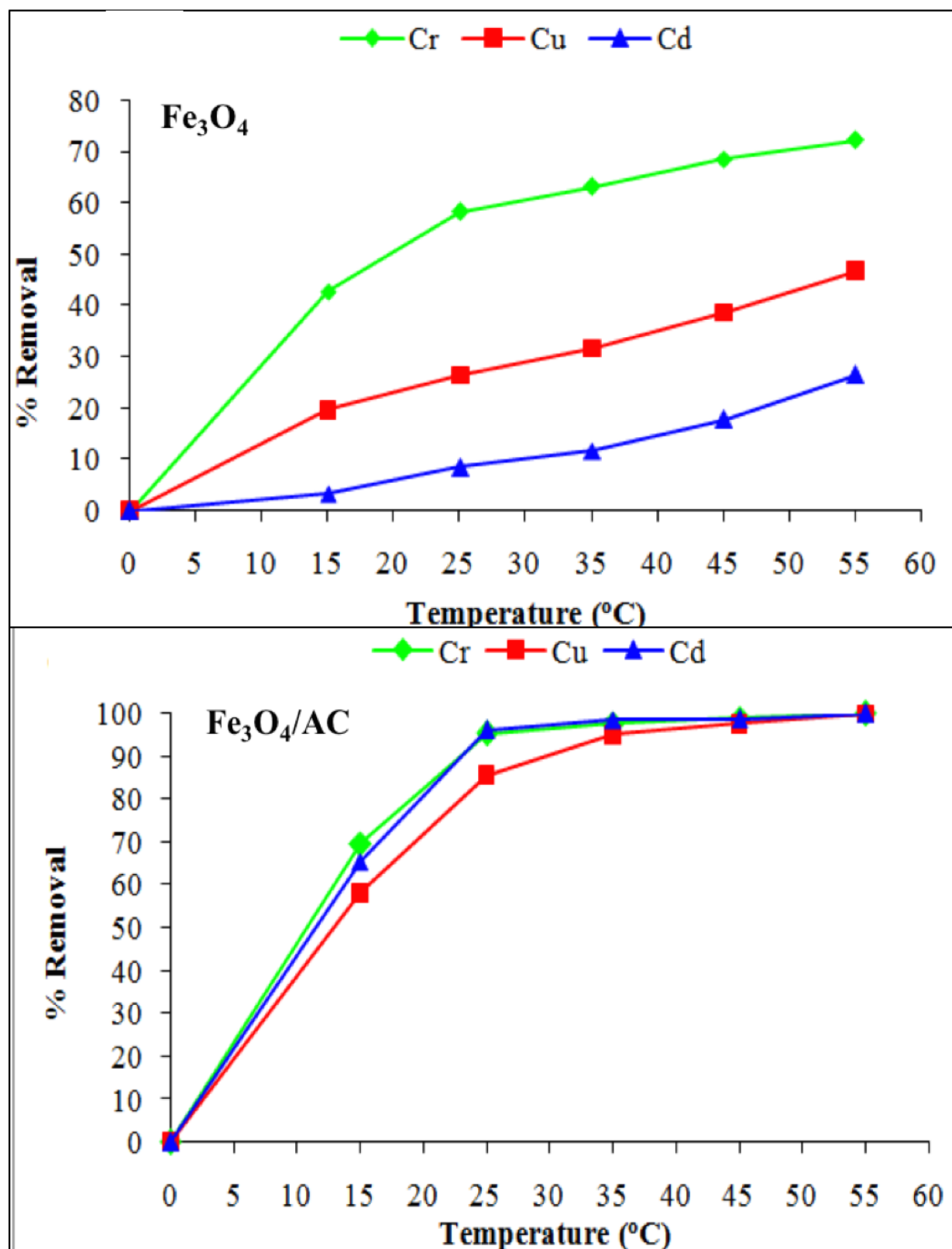
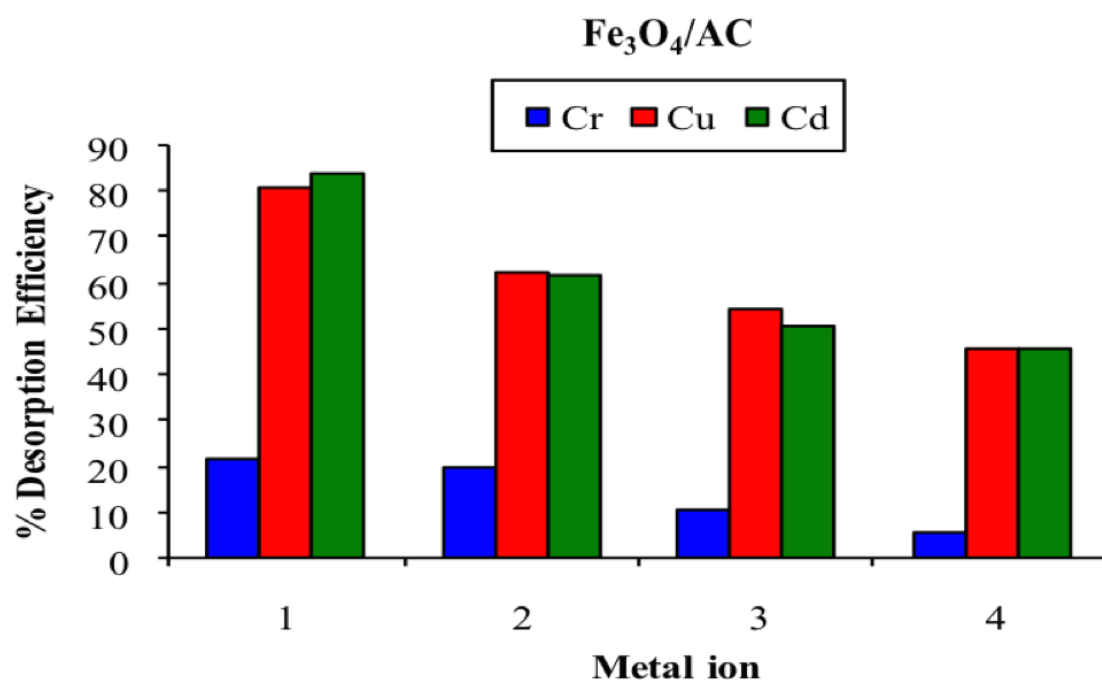
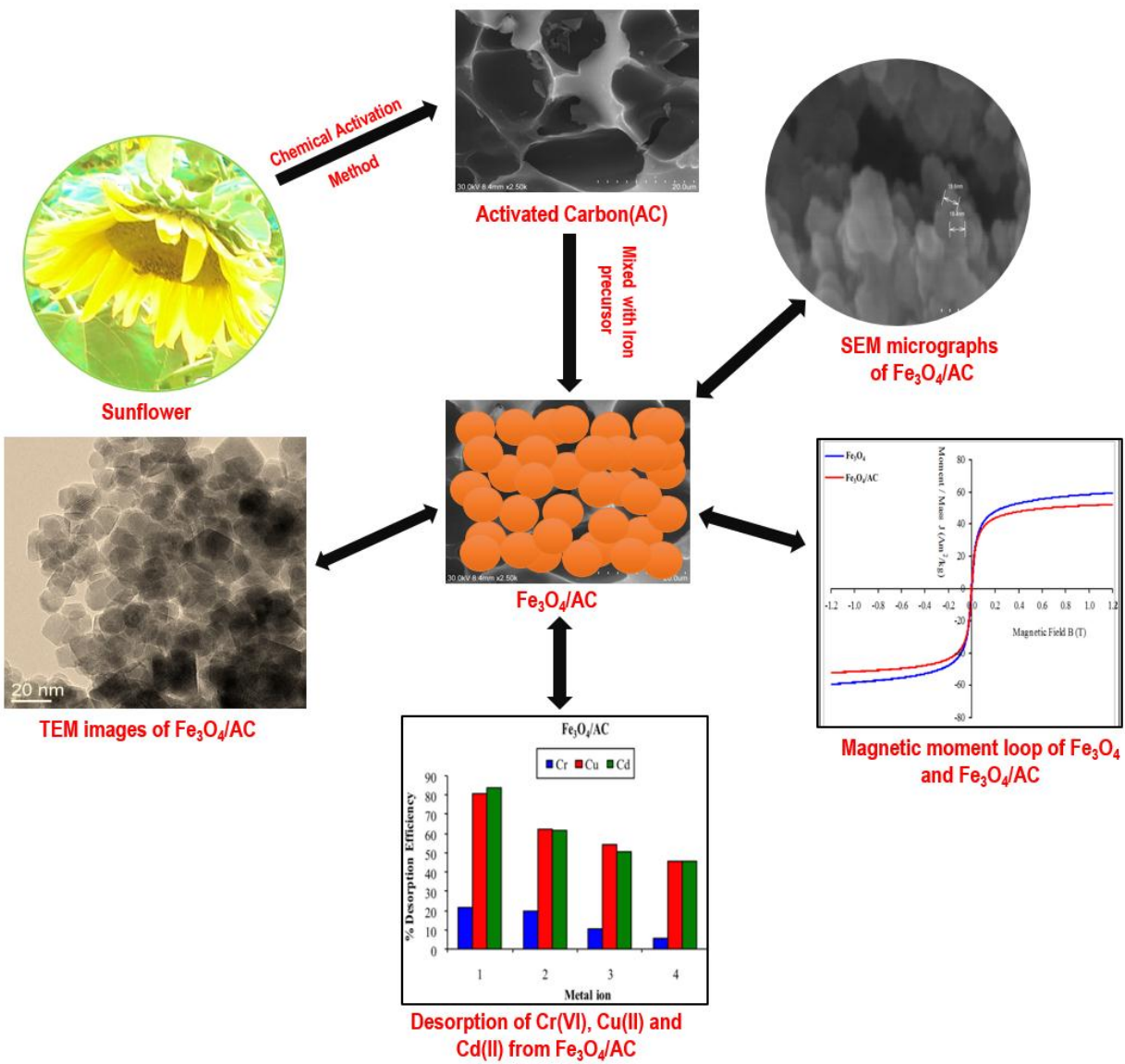


Fig.10

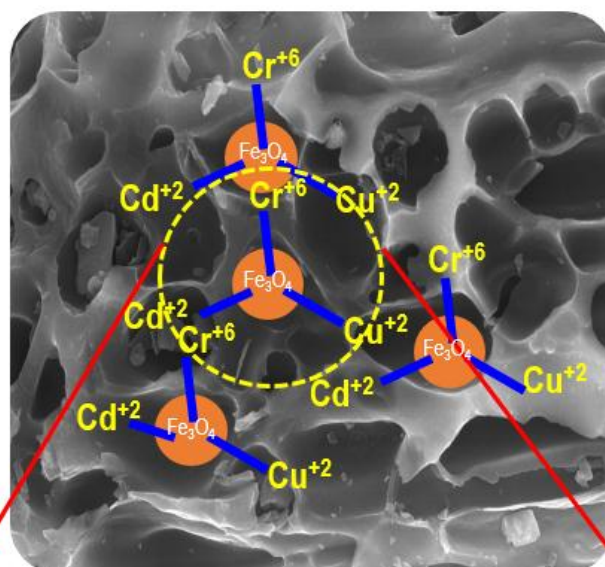


Accepted ma

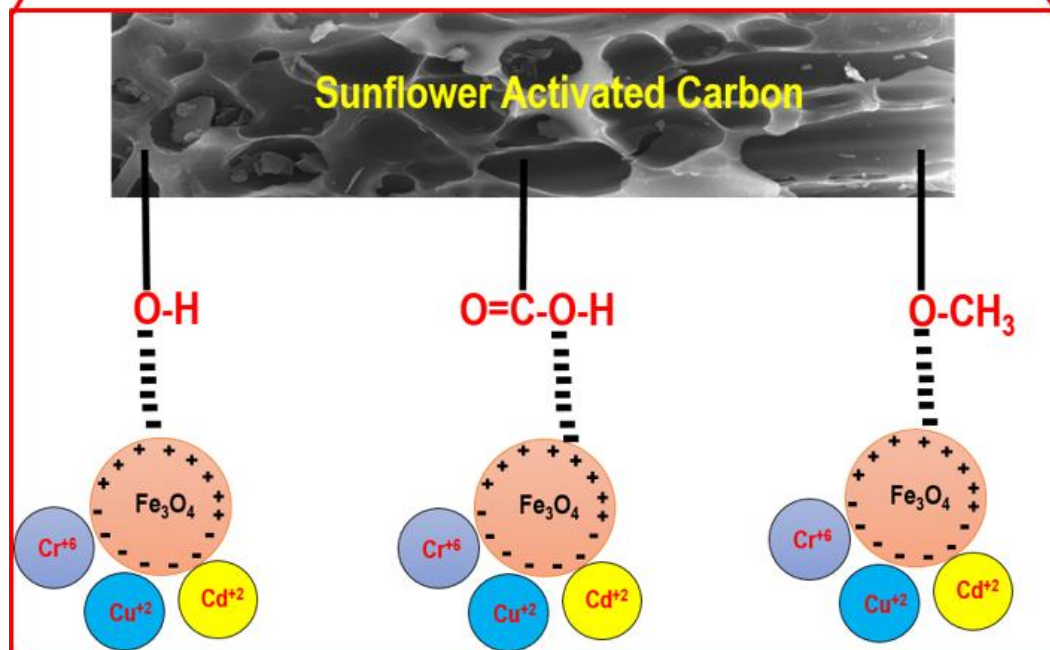
## Graphical Abstract



## Scheme I



Adsorption of Cr<sup>+6</sup>, Cu<sup>+2</sup> & Cd<sup>+2</sup> by iron oxide/activated carbon



Schematic illustration of Adsorption process for Cr<sup>+6</sup>, Cu<sup>+2</sup> & Cd<sup>+2</sup> by iron oxide/activated carbon